

**NON-NATIVE AGGREGATION OF ANTI-STREPTAVIDIN  
IMMUNOGLOBULIN GAMMA-1**

by

Na Young Kim

A thesis submitted to the Faculty of the University of Delaware in partial fulfillment of the requirements for the degree of Master of Chemical Engineering

Spring 2012

© 2012 Na Young Kim  
All Rights Reserved

**NON-NATIVE AGGREGATION OF ANTI-STREPTAVIDIN  
IMMUNOGLOBULIN GAMMA-1**

by

Na Young Kim

Approved: \_\_\_\_\_  
Christopher J. Roberts, Ph.D.  
Professor in charge of thesis on behalf of the Advisory Committee

Approved: \_\_\_\_\_  
Norman J. Wagner, Ph.D.  
Chair of the Department of Chemical and Biomolecular Engineering

Approved: \_\_\_\_\_  
Babatunde A. Ogunnaike, Ph.D.  
Interim Dean of the College of Engineering

Approved: \_\_\_\_\_  
Charles G. Riordan, Ph.D.  
Vice Provost for Graduate and Professional Education

## ACKNOWLEDGMENTS

First, I would like to thank my research advisor, Dr. Christopher Roberts. His insights, encouragements, and patience were indispensable in the completion of this thesis. I would also like to thank the members of the Roberts' group for the many helpful discussions, and the general willingness to lend a hand whenever any trouble arose in the lab. In particular, Becky Kalman provided immense amounts of guidance and training that I could not have done without.

Additionally, I would like to thank our collaborators at Amgen (especially Dr. Richard Remmele, Dr. Dingjiang Liu, and Dr. Vladimir Razinkov) and University of Virginia (Dr. Erik Fernandez and Shin Ahn) for the many helpful conversations and suggestions. Also, our collaborators at Amgen always made sure we had enough supply of protein, which made the process of experimentation that much smoother.

I also greatly appreciate the support of my parents and friends. My parents have been a constant source of encouragement, even from across the country. My friends and roommates are thanked for keeping everything in perspective and helping relieve stress so many times in the past two years.

## TABLE OF CONTENTS

LIST OF TABLES .....	vi
LIST OF FIGURES.....	vii
ABSTRACT.....	ix

### Chapter

1	INTRODUCTION.....	1
1.1	Motivation .....	1
1.2	Rates of non-native aggregation.....	2
1.3	Mechanisms of aggregation and aggregate types that result.....	3
1.4	Reversible phase separation of aggregates.....	5
1.5	Aggregation-prone domain of IgG1 .....	6
1.6	Anti-streptavidin IgG1 .....	6
1.7	Objectives of the thesis .....	7
2	MATERIALS AND METHODS .....	9
2.1	Solution preparation .....	9
2.2	Size exclusion chromatography with in-line multi-angle light scattering (SEC-MALS).....	10
2.3	Differential scanning calorimetry (DSC) .....	11
2.4	T <sub>2h</sub> measurements.....	11
2.5	Static Light Scattering (SLS) to assess colloidal monomer interactions	12
2.6	State diagram.....	14
2.7	pH titrations for pre-formed aggregates .....	15
2.8	Far-UV Circular Dichroism (CD) .....	16
2.9	Intrinsic fluorescence (FL).....	18
2.10	Thioflavin T (ThT) binding fluorescence.....	19
3	RESULTS.....	20
3.1	Conformational stability by DSC.....	20
3.2	T <sub>2h</sub> response surface .....	24
3.3	Colloidal interactions by SLS .....	30
3.4	Qualitative aggregation mechanism as function of pH and NaCl concentration .....	32

3.5	Reversible aggregate phase separation.....	40
3.6	Structural changes with aggregation .....	44
3.6.1	Circular dichroism (CD).....	44
3.6.2	Intrinsic fluorescence (FL).....	47
3.6.3	ThT binding fluorescence.....	49
3.6.4	Qualitative comparison of structural assays.....	51
4	DISCUSSION .....	53
4.1	Aggregation rates show opposite correlations with T <sub>m</sub> and G22 vs. pH and [NaCl].....	53
4.2	Combined pH and NaCl effects on aggregation mechanism and formation of insoluble aggregates.....	57
4.3	Structural changes from aggregation and their possible effect on mechanism of aggregation .....	59
5	CONCLUSIONS AND FUTURE WORK .....	62
	REFERENCES.....	64

## LIST OF TABLES

<b>Table 2.1</b>	<b>Selected isothermal incubation conditions for creating aggregates used for structural characterization (Figs. 3.13 – 3.15)..</b>	<b>18</b>
<b>Table 3.1</b>	<b>Estimated regression coefficients table for the T<sub>2h</sub> response surface design of experiments (from Minitab®).</b>	<b>26</b>
<b>Table 3.2</b>	<b>Qualitative ranking of structural changes of aggregates formed through different growth mechanisms as measured using different techniques.</b>	<b>52</b>

## LIST OF FIGURES

<b>Figure 3.1</b>	<b>Excess heat capacity from differential scanning calorimetry (DSC).</b> .....	21
<b>Figure 3.2</b>	<b>Partial DSC scans of 1 mg/mL antiSA in pH 4, 100 mM NaCl.</b> .....	23
<b>Figure 3.3</b>	<b>Representative plot of fraction of monomer remaining in solution (from SEC) after two-hour isothermal incubation at various temperatures for 1 mg/mL samples at pH 6, 0 mM NaCl.</b> ..	25
<b>Figure 3.4</b>	<b>Contour plot of <math>T_{2h}</math> (indicated by labels and color code) as a function of pH and added NaCl concentration, based on a face-centered cube response-surface DOE (see main text for additional details).</b> .....	27
<b>Figure 3.5</b>	<b>Summary of pH and salt effects on aggregation rates, conformational stability, and colloidal interactions.</b> .....	29
<b>Figure 3.6</b>	<b>Representative static light scattering data with Equation 2.1 fitted to the data.</b> .....	31
<b>Figure 3.7</b>	<b>Representative size exclusion chromatograms of different isothermal aggregation mechanisms overlaid with molecular weight data from in-line multi angle light scattering.</b> .....	34
<b>Figure 3.8</b>	<b>Representative plots (<math>M_w^{tot}/M^{mon}</math> vs. <math>(1-m)^2</math>) of four aggregation mechanisms observed at different solution conditions.</b> .....	36
<b>Figure 3.9</b>	<b>State diagram of aggregation mechanism as a function pH and NaCl concentration.</b> .....	39
<b>Figure 3.10</b>	<b>Representative pH titration at room temperature of initially soluble aggregates.</b> .....	41
<b>Figure 3.11</b>	<b>Reversible phase transitions of aggregates with various concentrations of added NaCl.</b> .....	42
<b>Figure 3.12</b>	<b>Overlay of the boundary between soluble and phase-separated aggregates (x symbols and dashed line) on the state diagram of qualitative aggregation mechanisms.</b> .....	43

<b>Figure 3.13</b>	<b>Circular dichroism (CD) spectra for monomer and aggregates at four different conditions corresponding to different regions of the aggregation mechanism state diagram (Figure 3.9).</b>	<b>46</b>
<b>Figure 3.14</b>	<b>Intrinsic fluorescence spectra showing monomer (solid) and aggregate (dashed) at four different conditions corresponding to different growth mechanisms.</b>	<b>48</b>
<b>Figure 3.15</b>	<b>[Top] Thioflavin T (ThT) fluorescence spectra showing negligible binding to monomer (solid curves) and significant binding to aggregates (dashed curves) at the four conditions corresponding to Figure 3.9.</b>	<b>50</b>
<b>Figure 4.1</b>	<b>Comparison of interpolated <math>T_{2h}</math> values from the response surface versus <math>T_m</math> values corresponding to those in Figure 3.1.</b>	<b>56</b>

## ABSTRACT

Global aggregation behavior of a model IgG1 protein, anti-streptavidin (antiSA), was characterized as a function of pH and [NaCl] in acidic conditions. The relative rate of aggregation as illustrated by  $T_{2h}$  (temperature at which isothermal incubation resulted in an aggregation half-life of two hours), and mechanisms of aggregation at the different solution conditions were monitored. It was found that relative rate of aggregation is strongly influenced by conformational stability of the protein but generally independent of colloidal interactions. A state diagram of aggregation mechanisms suggested that the mechanism of aggregate growth, and thus the resulting aggregate type, is strongly dependent on electrostatic, inter-molecular interactions. When this state diagram was overlaid with a phase diagram from reversible phase transition studies, it was found that there was a strong correlation between the two, suggesting that the formation of insoluble aggregates from kinetic and thermodynamic means are by the same or similar mechanisms. Several structural assays (far-UV CD, and fluorescence (intrinsic and ThT binding)) were used to analyze the changes in secondary and tertiary structure due to aggregation by the various mechanisms. It was found that ThT bound equally to all types of soluble aggregates, suggesting amyloid fibril formation at all conditions observed. However, the other assays showed varying amounts of structural changes depending on pH and

NaCl concentrations, with conditions that have largest inter- and intra- molecular repulsions having the largest change in structure. This suggested that a combination of conformation change and electrostatic interactions may influence the type of aggregates that form via thermal stress.

## Chapter 1

### INTRODUCTION

#### 1.1 Motivation

Monoclonal antibodies (mAbs) have become an increasingly important pharmaceutical product in the past two decades or more, due to their relatively specific interactions and utility in many applications, such as controlling and diagnosing diseases.<sup>1,2</sup> As with other therapeutic protein products, these antibodies are prone to both chemical and physical degradation pathways, of which nonnative aggregation is among the most common.<sup>3</sup> Aggregation must be minimized in the final drug product for a variety of reasons. Aggregates may lead to loss of efficacy in the final product, and impact marketability and pharmaceutical elegance.<sup>4,5</sup> In addition, aggregates raise concerns regarding possible immunogenic responses.<sup>6-9</sup> It has been suggested that the severity and type of immunogenic response (if any) for protein aggregates depends on the amount, size, and type of aggregate in solution.<sup>10,11</sup>

Nonnative aggregation can occur at many of the steps in the development and production process of therapeutic products, at least in part because a number of different stresses can promote aggregate formation. These include low pH needed for viral inactivation, elevated temperatures, freezing and thawing of bulk solutions, contact with manufacturing, container/closure, or delivery device materials, and

agitation.<sup>3,4,12</sup> Any of these stresses can, in principle, increase the population of partially or fully unfolded monomers that are often implicated as key intermediates along non-native aggregation pathways.<sup>10,13–16</sup>

Once formed, non-native aggregates (hereafter simply referred to as aggregates) are typically irreversible under the conditions in which they were created, and require extreme sample conditions to dissociate them.<sup>16,17</sup> This may be due, at least in part, to conformational changes that accompany aggregation. Aggregates of therapeutic proteins have been found to contain increased amounts of intermolecular beta sheet structures,<sup>14,16,18–20</sup> although it is not always clear how much or what particular structural changes are required within a given protein in order to facilitate aggregation.<sup>1</sup> Because aggregation is typically irreversible and often under kinetic control, the pathway(s) by which aggregates form can be important in controlling the size, morphology, and/or underlying structure of proteins within the resulting aggregates.

## **1.2 Rates of non-native aggregation**

Predicting and controlling aggregation rates remains a challenging task, as many factors can affect the process. In bulk solution, important formulation variables include pH, ionic strength, salt or buffer type, and the presence and concentration of different excipients. At a minimum, changes to any of these variables can affect protein conformational stability and/or inter-protein interactions.<sup>16,21–23</sup>

Conformational stability can be an important factor in determining the rates of aggregation, because partially unfolded monomer states have been found to be the reactive species in nonnative aggregation.<sup>10,13-16</sup> On the other hand, the intermolecular interactions influence how these reactive species interact with one another, as well as with aggregates.<sup>5,16,22</sup> In addition to the rate of aggregation, these formulation variables also influence the mechanism of aggregation, and thus the resulting type of aggregate.

### **1.3 Mechanisms of aggregation and aggregate types that result**

Extensive studies in the past have demonstrated that changes in solvent conditions can cause the same protein to form aggregates of different sizes, morphologies, and/or underlying secondary structures. Li and coworkers showed that the mechanism of aggregate growth varied as a function of pH and [NaCl] for a globular protein, alpha-Chymotrypsinogen A (aCgn).<sup>24</sup> By relating the mechanism of aggregation with colloidal interactions, they observed a semi quantitative relationship between  $B_{22}$  and aggregation pathway.<sup>24</sup> In their study, the different aggregation pathways led to various types of aggregates, such as soluble versus insoluble aggregates, and low versus high polydispersity.<sup>24</sup> Similarly, Hoyer and coworkers studied the aggregation behavior of alpha-Synuclein in various pH and salt concentrations.<sup>25</sup> They found aggregates of fibrillar, helical twist, and amorphous morphologies depending on the solution conditions.<sup>25</sup> A study by Krebs and

coworkers on the aggregation of beta-Lactoglobulin across a range of pH values suggested that while aggregates of different morphologies formed depending on the distance from pI, there was an underlying amyloid-like fibril structure at all pH conditions.<sup>18</sup> These studies empirically show that pH and ionic strength can strongly influence the qualitative characteristics of aggregates that form.

In less extensive studies, IgG1 antibodies have been shown to change the aggregate growth pathway(s) based on changes in pH, and to a lesser extent in [NaCl]. In monitoring isothermal aggregation of an IgG1 at three different pH values, Brummitt and coworkers found that all three conditions resulted in different aggregate mechanisms.<sup>26</sup> Sahin and coworkers observed the aggregation behavior of four IgG1 antibodies at various pH values at two ionic strength conditions.<sup>11</sup> They found different aggregation mechanisms, similar to the ones that Li et al. observed for aCgn, at the different solution conditions.<sup>11</sup> Also, in a high throughput study, where only one time point in isothermal aggregation was measured, Li and coworkers found that three mAbs (one IgG1 and two IgG2 antibodies) showed strong dependence of aggregation mechanism on solution pH and ionic strength.<sup>27</sup> However, a systematic and more global study of the aggregation pathways for an IgG antibody have not yet been reported as a function of pH and salt content. The present work, to the best of our knowledge, includes the most systematic study to date of the global aggregation behavior of an IgG1.

#### 1.4 Reversible phase separation of aggregates

In addition to the kinetically controlled growth of aggregates, recent studies have shown that aggregates can undergo reversible phase transitions between a soluble or dissolved (molecularly dispersed) state in aqueous solution, and a macroscopically condensed or concentrated phase.<sup>26,28,29</sup> This condensed phase appears as visible haze in experimental conditions, and is referred to as insoluble aggregates in this study. The phase transition may be analogous to a liquid-liquid phase separation that occurs for native or folded (monomer) proteins, but is different in that the phase separating species are the irreversible aggregates. In fact, under the same conditions, the native or folded proteins remained dissolved in solution. An extensive study of this phase behavior of aCgn aggregates was recently performed as a function of pH, ionic strength, and salt type.<sup>28</sup> All three of these variables had an impact on the phase separation of aggregates that were soluble as formed kinetically, indicating that a complex mechanism is involved in the phase behavior.<sup>28</sup> A less extensive study indicated that this phase behavior is possible for an IgG1 as a function of pH as well.<sup>26</sup> In the case of an IgG2, it has also been found that temperature is a variable in aggregate phase behavior.<sup>29</sup> Although an extensive analysis of the phase behavior of an IgG1 is beyond the scope of this work, it has been explored as a function of pH and [NaCl].

## 1.5 Aggregation-prone domain of IgG1

In addition to the various types of aggregates that can form, because mAbs are multidomain proteins, it has also been of interest to determine if there is a particular domain that is especially prone to aggregation. Some studies have determined that the least conformationally stable domain (CH<sub>2</sub>) is the aggregation-relevant domain.<sup>30,31</sup> On the other hand, there have been examples that show that the Fab domain may be the aggregation prone domain, despite the fact that it is more conformationally stable.<sup>10,32</sup> This has been briefly observed in this report as well.

## 1.6 Anti-streptavidin IgG1

The protein studied in this thesis is anti-streptavidin (antiSA) IgG1. As with other IgG1 antibodies, it is a multidomain protein composed of two identical Fab domains and an Fc domain, which is composed of the CH<sub>2</sub> and CH<sub>3</sub> domains.<sup>1</sup> This Fc has a constant sequence among all IgG1 antibodies.<sup>1</sup> As a model antibody developed for fundamental research, it has been utilized in other aggregation studies as well. In combination with the IgG2 variant of the antiSA, it has been found that IgG1 is less aggregation prone than IgG2.<sup>33</sup> Through the same study, it was suggested that disulfide bond formation has an important role in aggregation at neutral pH.<sup>33</sup> AntiSA IgG1 was also found to aggregate as a result of adsorption to stainless steel.<sup>34</sup> Silicone

oil and agitation was found to have a synergistic effect in creating aggregates of antiSA IgG1 with a high sensitivity to colloidal stability and presence of surfactants.<sup>35</sup> These studies show that antiSA is a valid model system, as it is sensitive to the different stress conditions that mAbs have been known to aggregate under.

## **1.7 Objectives of the thesis**

The main objective of this thesis was to characterize the factors influencing the relative rates of aggregation and types of aggregates that form for antiSA IgG1, as a function of pH and [NaCl] under accelerated (elevated temperature) conditions. The effects of intra- and inter-molecular interactions were inferred by observing the qualitative mechanism(s) of aggregate formation as a function of pH and [NaCl], as well as differences in monomer conformational stability and colloidal interactions, and structural differences in the resulting aggregates. In addition, reversible phase separation of initially soluble aggregates was characterized and quantitatively compared to the global aggregation behavior.

The remainder of the thesis is organized into chapters. Chapter 2 describes the experimental methods employed in observing the effects of pH and [NaCl] on the non-native aggregation of antiSA IgG1. The results of the various studies are presented in Chapter 3. These results are discussed in terms of how intra- and inter-molecular interactions may be influencing the global aggregation behavior of antiSA IgG1 in Chapter 4. Chapter 5 summarizes the conclusions of this study. The methods, results,

discussion, and conclusions presented in thesis are also presented as part of a manuscript that has been submitted for publication.<sup>36</sup>

## **Chapter 2**

### **MATERIALS AND METHODS**

#### **2.1 Solution preparation**

Purified anti-streptavidin (antiSA) IgG1 antibody, was provided by Amgen as a stock solution with approx. 30 mg/mL protein. All stock solutions were confirmed to be greater than 98% monomer by peak area in size-exclusion chromatography, with the only other detectable species being dimer (see also below). For buffer preparation, citric acid monohydrate (ACS grade; Fisher Scientific, Pittsburgh, Pennsylvania) and sodium chloride (ACS grade; Fisher Scientific) were dissolved in distilled, deionized water (Milli-Q filtration system with Quantum EX ultrapure organex cartridge; Millipore, Billerica, Massachusetts). All buffer concentrations were 5 mM unless otherwise noted. Buffers were pH adjusted using 5 M sodium hydroxide (Fisher Scientific), and filtered with 0.45  $\mu\text{m}$  pore size filters (Durapore® Membrane Filters; Millipore) prior to use. Protein samples were doubly dialyzed against a given buffer using Spectra/Por 7 dialysis tubing (10,000 Da molecular weight cutoff, Spectrum Laboratories, Rancho Dominguez, California) and filtered (Millex® GV PVDF 33 mm, 0.22  $\mu\text{m}$  pore size, syringe driven filters; Millipore). Post-dialysis protein

concentration was determined using absorbance at 280 nm measured with a UV-Vis spectrophotometer (Agilent 8453 UV-Vis spectrophotometer; Agilent Technologies, Santa Clara, California). The final protein concentration was adjusted gravimetrically, as needed, using the corresponding dialysis buffer.

## **2.2 Size exclusion chromatography with in-line multi-angle light scattering (SEC-MALS)**

Size exclusion chromatography (SEC) measurements were conducted with a Waters (Milford, Massachusetts) Alliance 2695 Separations Module with a Tosoh Bioscience (Montgomeryville, Pennsylvania) TSK-Gel G3000SWxl column held at ambient conditions. Samples were placed in Waters HPLC vials with pre-slit vial caps, and were maintained at 4 °C in an autosampler compartment. The mobile phase was 0.5 (v/v)% phosphoric acid, 50 mM sodium chloride, pH 3.5, with a flow rate of 1 mL/min. Mobile phase was prepared as described previously.<sup>10</sup>

A Waters 2996 photodiode array detector, Wyatt (Santa Barbara, California) DAWN-HELEOS II multi-angle light scattering (MALS) detector, and Wyatt Optilab rEX refractive index detector were used in series, in conjunction with Empower™ software module (Waters). Integrated peak areas were used to quantify monomer fraction, as described below ( $T_{2h}$  determination). The value of the weight-average molecular weight ( $M_{w,i}$ ) at each  $i$ th one-second slice of the column eluate was determined using ASTRA V™ software (Wyatt Technology) based on the inline MALS and RI detectors. By integrating  $M_{w,i}$  across both the monomer and aggregate

peaks, the total weight-average molecular weight ( $M_w^{\text{tot}}$ ) was determined for a given sample, as described previously.<sup>37,38</sup> The monomer molecular weight ( $M^{\text{mon}}$ ) was calculated from the monomer control sample by integrating the monomer peak, excluding artifacts from the low-concentration tails of the peak. The MALS and refractive index detectors were temperature controlled at 25 °C.

### 2.3 Differential scanning calorimetry (DSC)

Differential scanning calorimetry (DSC) measurements were performed using a VP-DSC instrument (Microcal, Northampton, Massachusetts). Protein concentration was 1 mg/mL for all solution conditions. Temperature was scanned from 20 to 90 °C at a rate of 1 °C/min, with instrument thermal history and baseline determined through a series of buffer/buffer scans prior to a given protein/buffer scan. Raw data were used to calculate absolute heat capacity values based on standard corrections for the reference cell.<sup>39,40</sup> The low-temperature linear baseline of the native protein was subtracted from absolute  $c_p$  to obtain  $c_{p,\text{ex}}$ .

### 2.4 $T_{2h}$ measurements

For selected solution conditions,  $T_{2h}$  was determined using size exclusion chromatography (SEC, see also above). A series of 1 mg/mL protein samples were incubated isothermally at a range of temperatures for two hours in hermetically sealed HPLC vials, after which they were immediately quenched in an ice-water bath for at

least five minutes to arrest aggregation. Quenched samples were assayed by SEC with external standards (see above) to determine the monomer content, reported as the fraction ( $m$ ) relative to the initial monomer concentration. The values of  $m$  versus temperature ( $T$ ) were used to fit an empirical asymmetric sigmoidal function<sup>41,42</sup> so as to interpolate the temperature at which  $m = 0.5$ . This temperature is defined as  $T_{2h}$ .

$T_{2h}$  values interpolated from the fits at each of the experimental conditions were analyzed by a simple multi-variable regression to create a continuous response surface using Minitab<sup>®</sup> (Minitab Inc., State College, Pennsylvania). The multivariable regression was based on  $T_{2h}$  in terms of pH, [NaCl], and the product pH x [NaCl]. Higher order terms were also considered, but were not found to provide statistically significant improvements to the regression including the analysis of variance (ANOVA); see also Chapter 3.

## **2.5 Static Light Scattering (SLS) to assess colloidal monomer interactions**

Static light scattering experiments were performed using a Wyatt Calypso instrument with a Wyatt DAWN HELEOS-II multi-angle light scattering (MALS) detector and Wyatt Optilab rEX refractive index detector. A series of serial buffer dilutions were performed for each solution condition tested, with the average MALS signal recorded for each dilution. The starting concentration of protein was nominally 20 mg/mL (confirmed quantitatively by RI) for all conditions except pH 4, 0 mM NaCl, for which it was 10 mg/mL for reasons discussed below (see Chapter 3). Each

sample and buffer was filtered through a 0.22  $\mu\text{m}$  syringe filter prior to use in the Calypso. The refraction index increment ( $dn/dc$ ) was estimated as 0.186, and treated as effectively independent of solvent concentration for the purposes of these measurements.<sup>10,11</sup>

Averaged scattered intensities were confirmed as independent of scattering angle (not shown) and converted to excess Rayleigh ratios ( $R_{ex}$ ) using toluene as a reference, as described previously.<sup>11</sup>  $R_{ex}$  as a function of protein concentration ( $c$ ) was regressed using Eq. 2.1 to determine values of the apparent molecular weight ( $M_{w,app}$ ) and protein-protein Kirkwood Buff integral ( $G_{22}$ )<sup>43</sup> for each solvent condition tested. In Eq. 2.1  $K$  is a lumped constant, including the scattering geometry, ( $dn/dc$ ), and calibration against pure toluene. As noted elsewhere,<sup>43</sup> for practical purposes and in keeping with common practice,  $K$  was based on ( $dn/dc$ ) at constant pressure.

$$\frac{R_{ex}}{K} = M_w c + G_{22} c^2 \quad (2.1)$$

For readers unfamiliar with Eq. 2.1, it is a more general form for Rayleigh scattering as a function of protein concentration than the more restrictive and conventional form.<sup>43</sup> Unlike the conventional form used to regress Rayleigh scattering (e.g., as  $Kc/R_{ex}$  vs.  $c$ ), Eq. 2.1 is not restricted to highly dilute or weakly attractive / repulsive conditions, and is not restricted to cases where Donnan equilibria can be neglected.<sup>44</sup>  $G_{22}$  is a quantitative measure of protein-protein interactions that is conceptually similar to the more familiar second osmotic virial coefficient  $B_{22}$ ,<sup>43</sup>

except that it carries the opposite sign as  $B_{22}$  and in the limit of low  $c$  it has double the magnitude (see also Chapters 3 and 4).

In order to provide values of  $G_{22}$  relative to a reasonable reference state, reported  $G_{22}$  values were scaled by the value for idealized hard-sphere (HS) proteins, as described elsewhere.<sup>43</sup> The reduced values ( $G_{22}^* = -G_{22} / 2B_{22,HS}$ ) are numerically equivalent to reduced  $B_{22}$  values ( $B_{22}^* = B_{22} / B_{22,HS}$ ) in the limit of low  $c$  and/or conditions of weakly repulsive or attractive conditions; but  $G_{22}^*$  is more general than  $B_{22}^*$ , in that it is applicable at higher  $c$  and under arbitrarily strong repulsive or attractive conditions.<sup>43</sup>

## 2.6 State diagram

Concentrated stock protein solutions were prepared by dialysis against buffers at pH 4, 5, or 6, as described above. After dialysis, protein stock solutions were diluted to 1 mg/mL using a combination of the dialysis buffer and a corresponding buffer in which 2 M NaCl was dissolved. The stock protein solution and the buffers, with and without added NaCl, were combined gravimetrically to reach the desired concentration of NaCl. Because NaCl was added after pH adjustment, in some cases this resulted in final pH values (tested independently) that were slightly lower than the no-added-NaCl samples, due to shifts in buffer pKa at high ionic strengths.

A qualitative state diagram was constructed by categorizing what type of aggregation mechanism was observed as a function of pH and added NaCl (all 5 mM

citrate buffer), during isothermal aggregation at elevated temperatures similar to those determined from the  $T_{2h}$  surface. Aggregation was monitored by SEC-MALS and visible observation as a function of incubation time at elevated temperatures; precise temperature values were adjusted as a function of pH and [NaCl] so as to keep experimental time scales less than a few hours to achieve one to two half lives of monomer loss (for most cases). After quenching on an ice-water bath, each sample was centrifuged at nominally 10,000 g for a minimum of five minutes to remove any insoluble aggregates from solution, and the supernatant was assayed on SEC-MALS as described above. Samples were stored and monitored (SEC-MALS and visible observation) under refrigerated conditions to confirm that no detectable dissociation or further aggregation occurred on time scales of days, after initial incubation at elevated temperature.

## **2.7 pH titrations for pre-formed aggregates**

Cloud points for otherwise soluble aggregates were determined based on pH titration with small volumes of concentrated base and/or acid, akin to those used previously for IgG or chymotrypsinogen systems.<sup>26,28</sup> Samples containing primarily small, soluble oligomers ( $M_w^{tot}/M^{mon} \approx 5$ ) and residual monomer (less than 10 % by SEC, not shown) were prepared by isothermally incubating 1 mg/mL protein solution at pH 4.5, 63 °C for 2.5 hours using the protocol described above for state diagram or  $T_{2h}$  determination. After quenching, this stock aggregate sample was diluted to

achieve 0.5 mg/mL (total aggregate basis) using a combination of the buffer and corresponding 2 M NaCl solution so to obtain new stock solutions at selected values of [NaCl]. For each of these stock solutions, 1.2 mL was placed into a disposable UV-Vis cuvette. Aliquots of less than 25  $\mu$ L of 0.05 M sodium hydroxide solution were used to then titrate pH, with percent transmission (%T) at 650 nm (Agilent 8453 UV-Vis Spectrophotometer) determined after each addition of NaOH. For the same sample, aliquots of less than 25  $\mu$ L of 0.05 M hydrochloric acid were used to back-titrate until a clear solution was recovered at acidic pH. The resulting sigmoidal profiles of %T versus pH were analyzed by interpolating the inflection point for the onset of haze or turbidity, based on the initial baseline and near linear regime for the steepest reduction in %T with pH (see also Chapter 3). Similar pH titrations with purely monomer controls (1 mg/mL) showed no detectable change in %T as a function of pH, confirming that the observed cloud points were not due to precipitation of monomer.

## **2.8 Far-UV Circular Dichroism (CD)**

Far-UV circular dichroism (CD) was used to assess the average secondary structure of aggregated samples and monomer controls at four solution conditions. The solution conditions and aggregate content are summarized in Table 2.1. Each protein sample was diluted to approximately 0.2 mg/mL after preparation as an aggregated solution as described above and in Table 2.1. A J-810 spectropolarimeter

(Jasco Inc., Easton, Maryland) was used to measure each spectrum, with the temperature held at 20 °C with a Jasco PTC-424S Peltier control unit. Three spectra were measured and averaged for each sample, using a 2 x 10 mm quartz cuvette. The corresponding buffer baseline was subtracted from each average spectrum, and the mean residue ellipticity (MRE) was calculated and reported in units of deg-cm<sup>2</sup>/dmol using the standard equation.<sup>10</sup> The monomer molecular weight was 142.2 kDa, and the total number of residues was 1322. Since each sample contained slightly different amounts of monomer, the MRE spectra were corrected by subtracting the monomer contribution, and normalizing on a per-unit-mass of aggregate to obtain the aggregate MRE spectra.

$$MRE_{\text{agg}} = \frac{MRE_{\text{tot}} - m \times MRE_{\text{mon}}}{(1 - m)} \quad (2.2)$$

In using the above equation, the  $m$  values were from SEC for a given sample, and it was assumed that monomers in the heat-treated samples have the same CD spectra as the monomer controls. This assumption was independently confirmed by comparing the CD spectra of unheated monomers with those from monomer samples that were heated to the temperature of interest for at least 10 minutes – sufficiently long to allow heating and at least some unfolding, but short enough to prevent measurable aggregation (confirmed by SEC) prior to quenching on an ice-water bath (data not shown).

**Table 2.1 Selected isothermal incubation conditions for creating aggregates used for structural characterization (Figs. 3.13 – 3.15).**

<b>Growth Mechanism</b>	<b>pH</b>	<b>[NaCl] (mM)</b>	<b>T (°C)</b>	<b>Incubation Time</b>	<b>Final % mon.</b>	<b>Final <math>M_w^{tot} / M^{mon}</math></b>
Nucleation Dominated (ND)	4	0	60	80 min	60	1.6
Chain Polymerization (CP)	5	20	60	48 hrs	40	9.9
Agg.-Agg. Condensation Polymerization (AP)	4	500	46	40 min	40	30
Condensation + Phase Separation	5	500	58	20 min	70	5
Precipitation / Phase Separation (PS)	6	0	67	180 min	60	--

## 2.9 Intrinsic fluorescence (FL)

Structural changes with aggregation were evaluated using intrinsic fluorescence. Each monomer control and aggregate sample was formed as described in Table 2.1 and the section above regarding CD spectroscopy. Each was diluted to approximately 0.2 mg/mL and placed into 2 x 10 mm quartz cuvettes. Using an ISS PC1 Spectrofluorimeter (Champaign, Illinois), the emission spectra were measured at 300 – 450 nm with excitation at 295 nm. The temperature was maintained at 20 °C using a Peltier controller (Quantum Northwest, Liberty Lake, Washington). At least three spectra were measured and averaged for each sample, prior to subtraction of the

corresponding buffer control. The monomer contributions to the aggregate emission spectra were subtracted, and then the spectra normalized on an aggregate mass basis, using Equation 2.2 but replacing MRE with the fluorescence intensity.

## **2.10 Thioflavin T (ThT) binding fluorescence**

Thioflavin T (ThT) binding was measured for the same samples as described in Table 2.1 and the preceding subsections, using the fluorescence instrumentation described above. Excitation was at 450 nm, with emission monitored between 460 and 600 nm. A stock solution of the dye was prepared by dissolving ThT in deionized water at a concentration of approximately 10 mM. This stock solution was diluted into a given 1 mg/mL protein solution (both monomer and aggregated samples) to obtain a 15:1 molar ratio of ThT to protein (monomer basis). A minimum of two spectra were measured at each condition, averaged, and buffer-baseline subtracted. As described for CD and FL spectra, residual monomer contributions for each ThT emission spectra were subtracted, and the aggregate spectra normalized on a per-mass of aggregate basis, using Equation 2.2, but replacing MRE with the emission intensity at a given wavelength.

## Chapter 3

### RESULTS

#### 3.1 Conformational stability by DSC

Relative conformational stability of antiSA IgG1 monomer was characterized as a function of pH and added NaCl through differential scanning calorimetry (DSC).  $c_{P,ex}$  versus temperature (T) is shown in Figure 3.1. As is expected from previous studies on the unfolding of an IgG1,<sup>45,46</sup> DSC scans showed a maximum of three unfolding events. At pH 4, the unfolding of each of the domains (Fab, CH<sub>2</sub>, and CH<sub>3</sub>) appeared distinctively as three individual endotherms with the second peak having the largest area. At pH 5 and pH 6, only one peak was obvious, with possibly a shoulder towards lower T for pH 5 conditions. At high temperatures, the aggregates precipitated at these higher pH solutions, resulting in strong exotherms in the VP-DSC. The full exotherms are not shown, for clarity of the remainder of the figure.

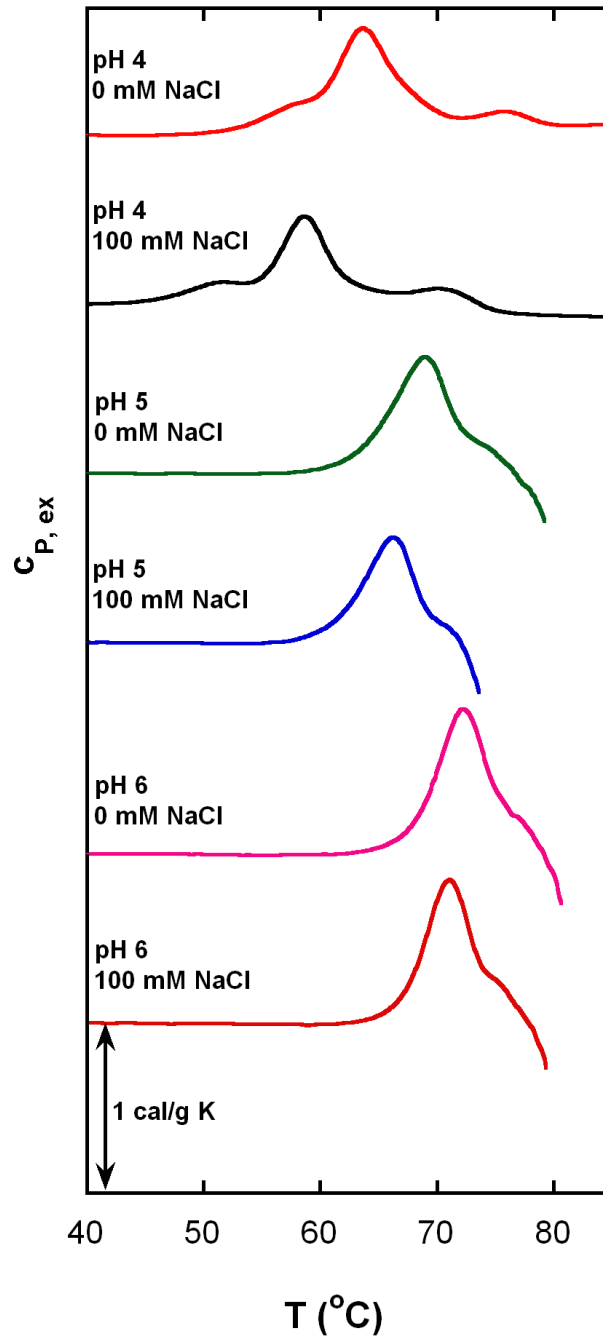


**Figure 3.1** Excess heat capacity from differential scanning calorimetry (DSC). The initial linear behavior of the  $c_p$  versus temperature was taken as the native monomer baseline, and this was subtracted out from the absolute  $c_p$  to calculate the  $c_{p,ex}$ .

For conditions where more than one peak was clearly distinguishable (pH 4), partial DSC scans were performed to determine reversibility of the unfolding events, using the same sample to repeatedly heat to successively higher  $T$  values. As shown in Figure 3.2, the first endotherm was reversible, even to the temperature of trough that is visible after this peak at pH 4, 100 mM NaCl. The second peak was not reversible to a significant degree. When the temperature was ramped to the initial rise in the second endotherm and then cooled again, there was a shift in the baseline and a significant loss in peak area during the rescan, indicative of aggregation.<sup>47,48</sup> According to previous studies on the conformational stability of IgG1s, the first, smaller peak is likely the unfolding of the CH<sub>2</sub> domain, and the second, larger peak is the unfolding of the Fab domain<sup>45,46</sup> at these acidic pH values. This would indicate that CH<sub>2</sub> unfolding is not sufficient to cause non-native aggregation at these conditions and time scales, but Fab unfolding is required. At higher pH values, there was only one visibly discernable endotherm, and this was irreversible in all cases tested (not shown).

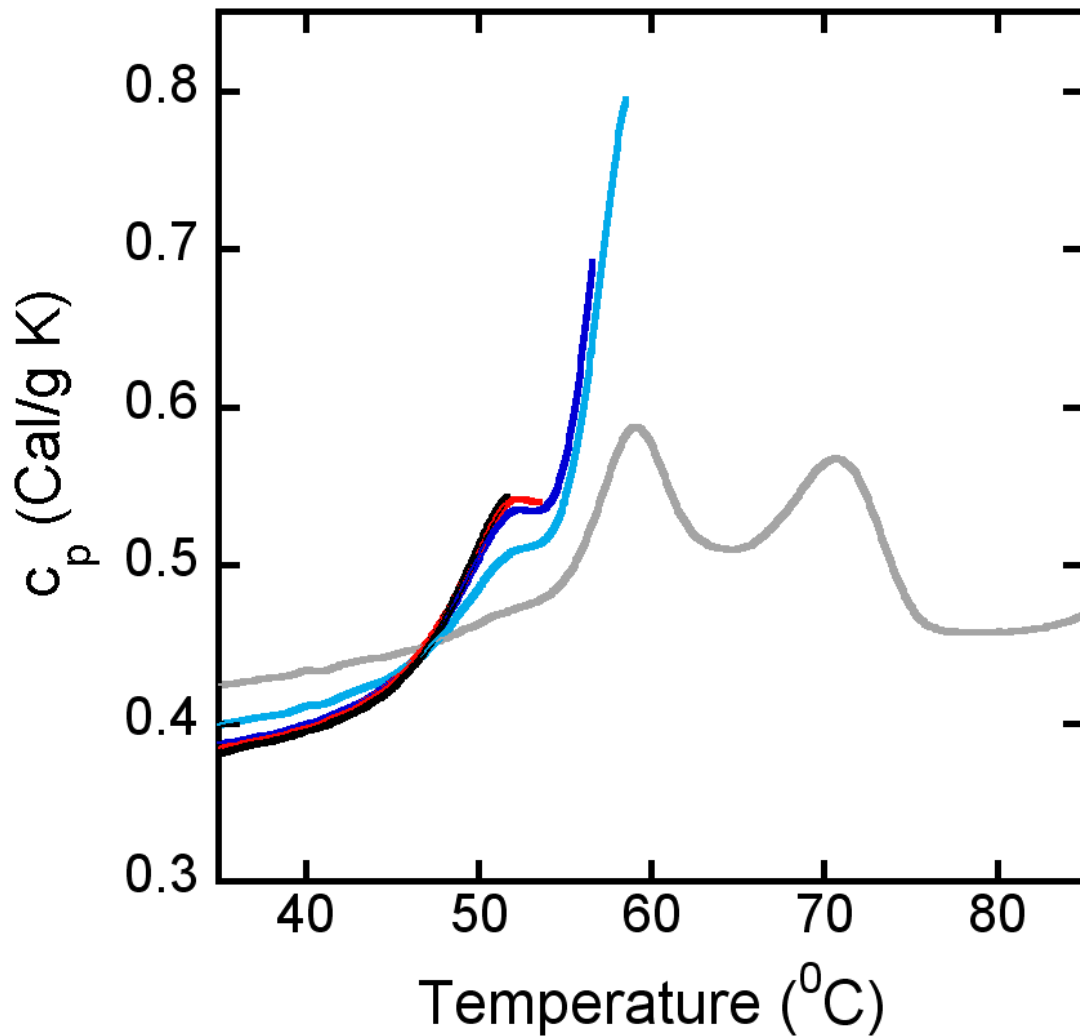


**Figure 3.2** Partial DSC scans of 1 mg/mL antiSA in pH 4, 100 mM NaCl. The dotted gray scan is the result of a single scan from 20  $^{\circ}\text{C}$  to 90  $^{\circ}\text{C}$  for a separate sample. The solid lines are the results of a single run, where the sample was scanned to the  $T_m$  of the first peak (black, 52  $^{\circ}\text{C}$ ), trough of the first peak (red, 54  $^{\circ}\text{C}$ ), part of the second peak (blue, 57  $^{\circ}\text{C}$ ),  $T_m$  of the second peak (light blue, 59  $^{\circ}\text{C}$ ), and all the way through (gray solid, 90  $^{\circ}\text{C}$ ). The system was cooled to 20  $^{\circ}\text{C}$  and held there for five minutes between each scan.

### 3.2 $T_{2h}$ response surface

The relative rates of aggregation as a function of pH and NaCl concentration were systematically probed through a response surface design of experiments (DOE). The response variable in this case was  $T_{2h}$ , the interpolated temperature at which the half-life of aggregation is 2 hours.  $T_{2h}$  was chosen because it is a relatively quick method to compare the rates of aggregation among conditions that have widely varying half-lives as a function of temperature, anywhere from seconds to weeks, across the full set of pH and [NaCl] of interest. Higher  $T_{2h}$  values correspond to longer half-lives if the aggregation reactions were carried out at the same temperature across the different conditions. Figure 3.3 shows an illustrative data set used to determine  $T_{2h}$  at pH 6, 0 mM NaCl. Each data point is the monomer fraction remaining in solution as calculated from size-exclusion chromatograph (SEC) after two hours of incubation at the corresponding temperature. The data points taken at a series of temperatures were used to fit an empirical sigmoidal model<sup>41,42</sup> for the purposes of interpolation (Eq. 3.1). The two adjustable variables are  $b$  and  $T_0$ .

$$m = \exp\left[-\exp(b(T - T_0))\right] \quad (3.1)$$

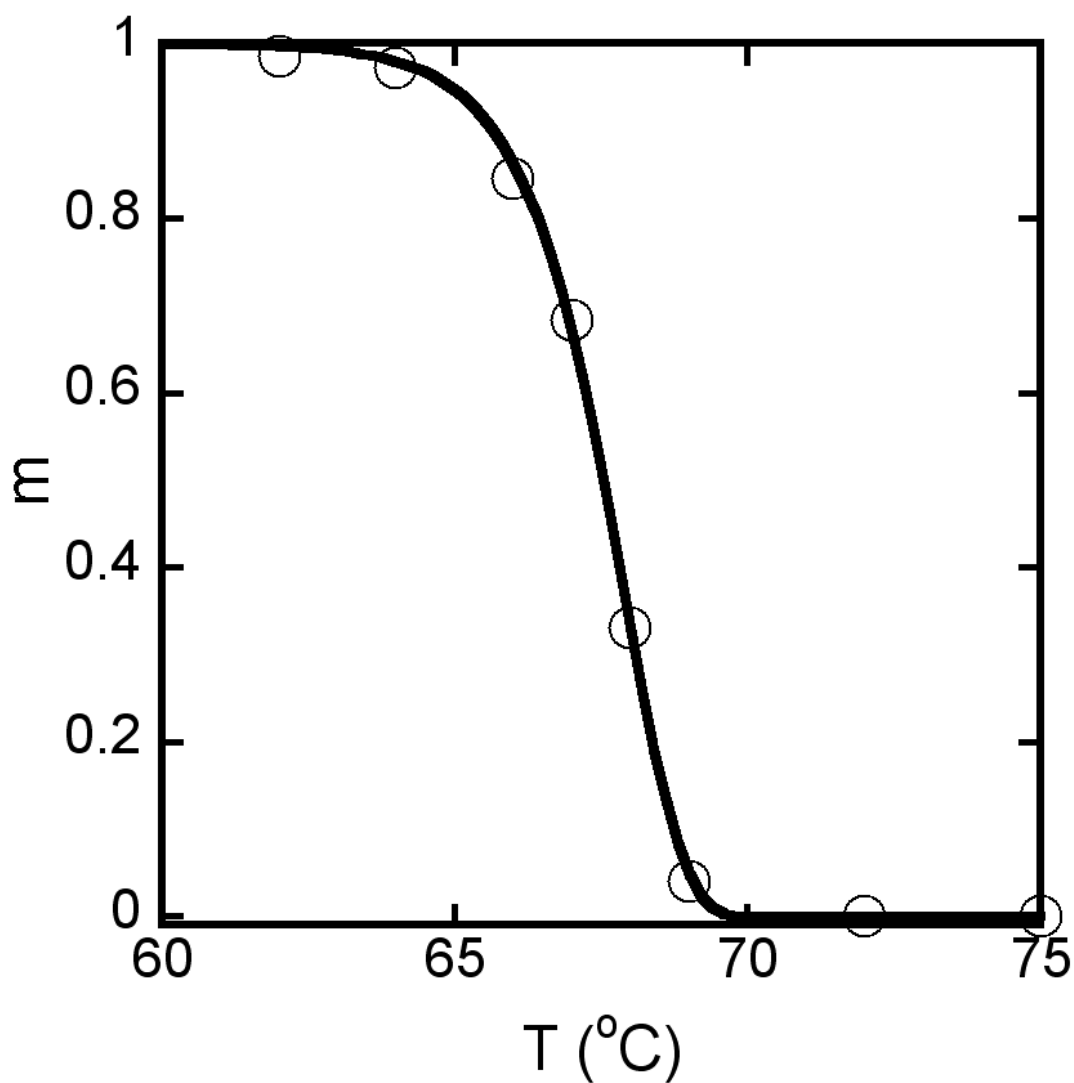


**Figure 3.3** Representative plot of fraction of monomer remaining in solution (from SEC) after two-hour isothermal incubation at various temperatures for 1 mg/mL samples at pH 6, 0 mM NaCl. The line is the sigmoidal model (Equation 3.1) fit to the data. The fits were used to interpolate  $T_{2h}$ , the temperature at which  $m = 0.5$  after incubation for 2 hr.

$T_{2h}$  values were determined at the solvent conditions indicated by the filled black circles in Figure 3.4. In order to determine the variability of the results, the center point was repeated five times, as per the standard face-centered cube response surface DOE protocol.<sup>49</sup> Minitab® was used to analyze the response surface DOE, which resulted in the following  $T_{2h}$  response function (Equation 3.1) and regression results (Table 3.1). Table 3.1 indicates that each of the individual terms and the interaction term are all statistically significant at a 95% confidence level with p-values lower than 0.05 for all terms. Additional interaction terms were also considered, but not deemed statistically significant, given the limited number of state points that were directly tested for  $T_{2h}$  values (not shown).

$$T_{2h} = a_0 + a_1(pH) + a_2(C_{NaCl}) + a_{12}(pH \times C_{NaCl}) \quad (3.2)$$

**Table 3.1 Estimated regression coefficients table for the  $T_{2h}$  response surface design of experiments (from Minitab®). The coefficients, standard error of each coefficient, t-score, and p-values are listed for each term.**

Source	Coefficient	SE Coef	T	P
Constant ( $a_0$ )	40	8	5.025	0.001
pH ( $a_1$ )	5	2	2.841	0.019
$C_{NaCl}$ ( $a_2$ )	-0.07	0.02	-2.819	0.020
pH x $C_{NaCl}$ ( $a_{12}$ )	0.012	0.005	2.344	0.044

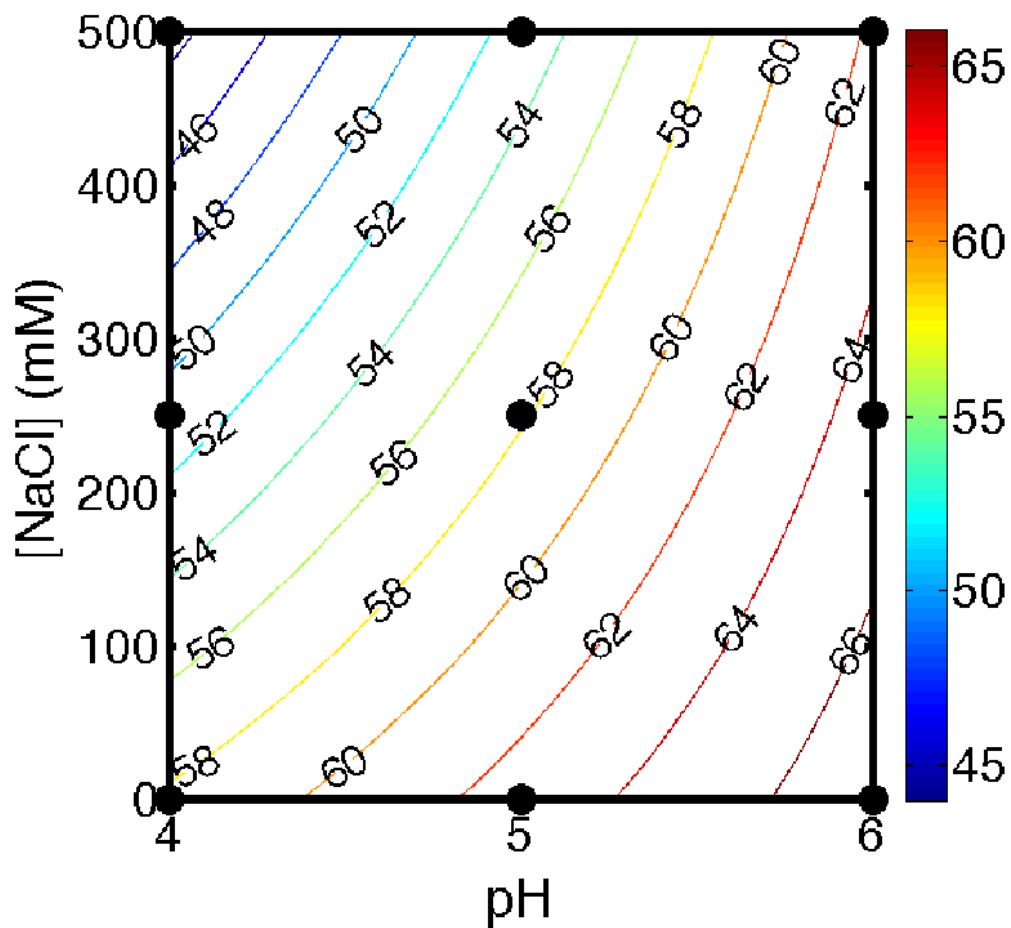


**Figure 3.4** Contour plot of  $T_{2h}$  (indicated by labels and color code) as a function of pH and added NaCl concentration, based on a face-centered cube response-surface DOE (see main text for additional details). The filled black circles represent conditions where data akin to the top figure were obtained for use in the DOE analysis.

Figure 3.4 shows the response surface contour plot of  $T_{2h}$  as a function of pH and [NaCl].  $T_{2h}$  varied between 44°C and 66°C in the design space. The lowest temperature was at the low pH and high NaCl concentration; the highest temperature was at the high pH and low NaCl concentration. This indicates that increasing pH and salt concentration have opposite effects on  $T_{2h}$ , and thus the relative rates of aggregation. Observing the spacing between the isotherms in the contour plot reveals that the relative aggregation rates are most sensitive to changing [NaCl] at low pH, and most sensitive to pH at high [NaCl]. Figure 3.5 summarizes the changes in  $T_{2h}$  from Figure 3.4, and the major endotherm (irreversible peak)  $T_m$  changes in Figure 3.1, as a function of pH and added NaCl.

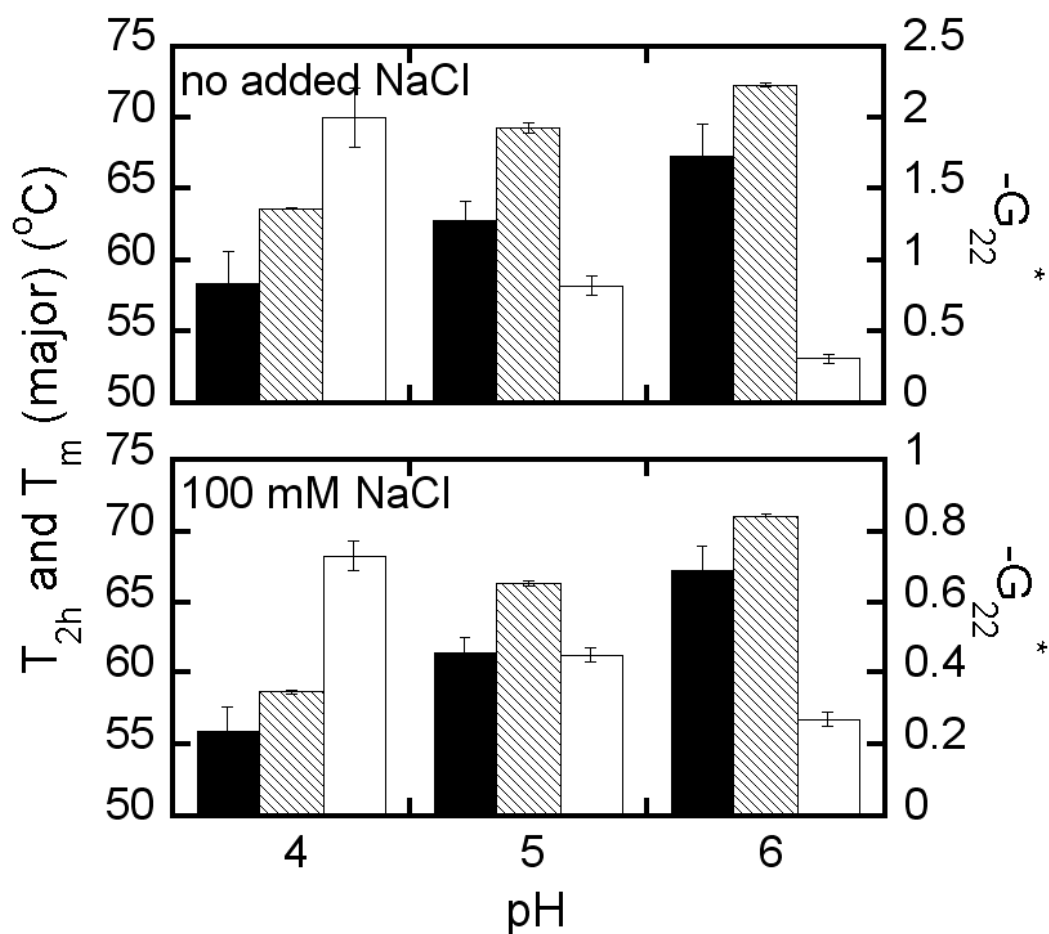


**Figure 3.5 Summary of pH and salt effects on aggregation rates, conformational stability, and colloidal interactions. The relative aggregation rates are represented by  $T_{2h}$  (black bars). Conformational stability is represented by  $T_m$  of the Fab or the major endotherm when those coincided (hashed bars). Colloidal interactions are represented with  $-G_{22}^*$  values (white bars).  $G_{22}$  values were calculated by fitting Equation 2.1 to static light scattering data. These  $G_{22}$  values were scaled by hard-sphere second virial coefficient ( $B_{22}^{HS}$ ) to obtain the non-steric net colloidal interactions between the monomers (see also, main text). The error bars are standard deviations in the replicate  $T_m$  measurements and in the nonlinear regression to determine  $T_{2h}$  and  $G_{22}$ .**

### 3.3 Colloidal interactions by SLS

Static light scattering (SLS) was implemented to study the effects of pH and added NaCl on the net colloidal interactions between native monomers at room temperature. The SLS data were analyzed using the model developed by Blanco et al., which shows that the protein-protein Kirkwood-Buff (KB) integral,  $G_{22}$ , is a more relevant measure of net colloidal interactions obtainable from light scattering than the traditional second osmotic virial coefficient ( $B_{22}$ ), especially at higher concentrations.<sup>43</sup> Figure 3.6 shows the representative fits to the data. In order to examine the magnitude of colloidal interactions relative to steric interactions,  $G_{22}$  was scaled with  $B_{22}^{HS} = (2/3)\pi\sigma_{HS}^3$ , where the  $\sigma_{HS}$  was estimated as 10 nm for this IgG1, based on typical hydrodynamic radii of IgG1 antibodies.<sup>26,50</sup> The scaled value is  $-G_{22}^* = -G_{22} / 2B_{22}^{HS}$ . These values are plotted as white bars in Figure 3.5, corresponding to the same conditions at  $T_{2h}$  and  $T_m$  reported in that figure. Generally, shifts to higher pH and lower NaCl concentrations corresponded to less repulsive (less negative)  $G_{22}^*$  values. None of the conditions were strongly attractive (see also, Chapter 4).

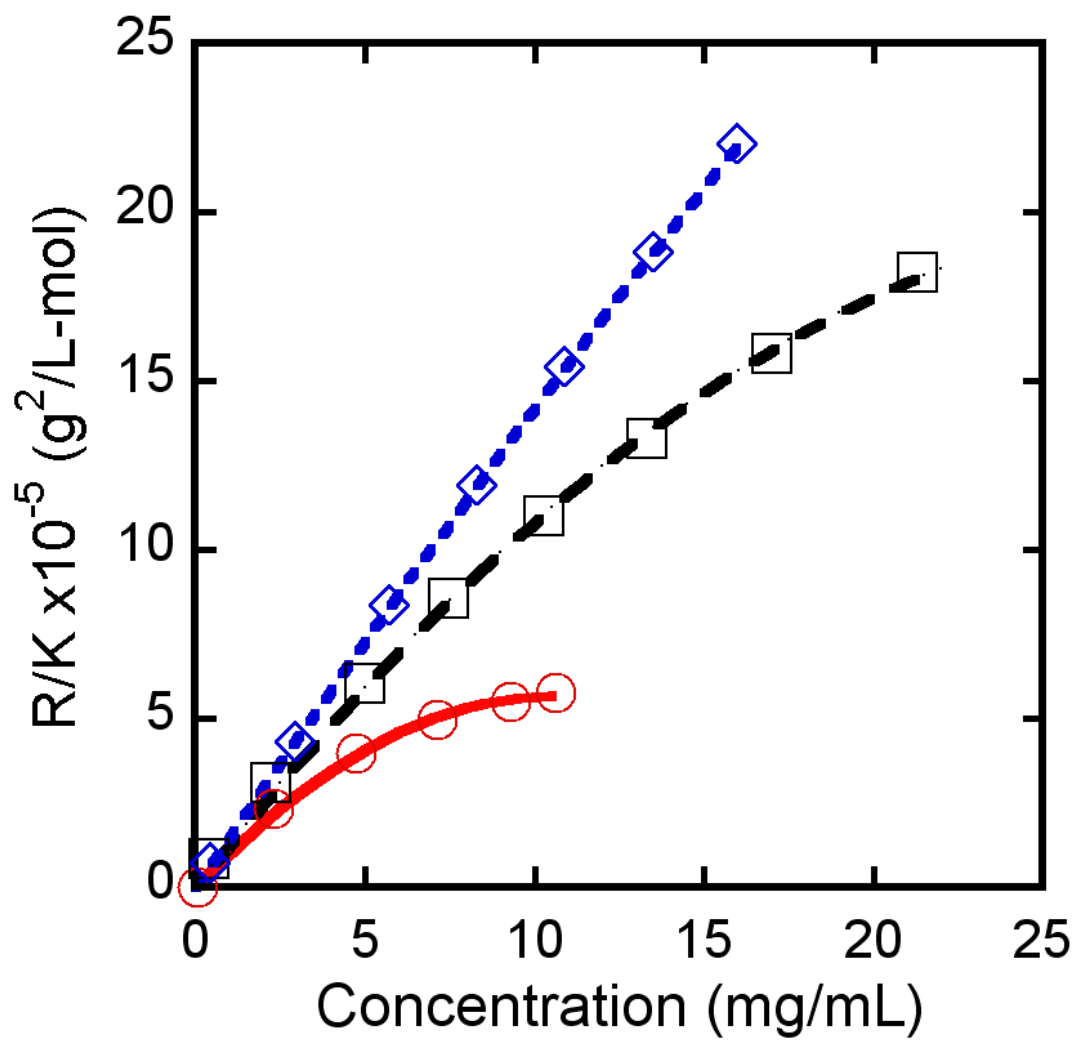


**Figure 3.6** Representative static light scattering data with Equation 2.1 fitted to the data. The data shown are samples with no added salt at pH 4 (red), pH 5 (black), and pH 6 (blue).

### 3.4 Qualitative aggregation mechanism as function of pH and NaCl concentration

The qualitative aggregate growth mechanisms were characterized at 1 mg/mL initial monomer concentration as a function of pH and NaCl concentration. The monomer fraction (SEC) and weight average molecular weight (inline MALS) were monitored for samples incubated isothermally at accelerated conditions (elevated temperature) for slightly longer than one half-life at a given pH and [NaCl]. The temperature of incubation varied between 46 °C and 67 °C at the different solution conditions. For practical reasons, the incubation temperatures were not chosen to align exactly with the  $T_{2h}$  values in Figure 3.4, but rather they were semi-quantitatively in keeping with Figure 3.4. It was also difficult to choose a single temperature to monitor aggregation at such a wide range of conditions, for the reasons noted above regarding Figure 3.4, and therefore a select set of temperatures were chosen to allow the largest number of samples to be incubated at the same temperature while retaining a pragmatically reasonable half life for this study.

Figure 3.7 shows representative SEC chromatograms overlaid with molecular weight information from the inline MALS for three conditions that had distinguishable aggregation growth mechanisms. Under the SEC conditions utilized, monomer eluted at approx. 7.9 minutes, dimer at approx. 6.8 minutes, trimer at approx. 6.3 minutes, and aggregates larger than trimers coeluted at approx. 5.7 minutes. Figure 3.7A shows

a representative condition (pH 4, zero added NaCl) where nucleation dominated and growth was slow. Under these conditions, aggregates only grew to be small oligomers, on average. There was a significant amount of dimer accumulation throughout the aggregation reaction, as seen from the chromatograms.

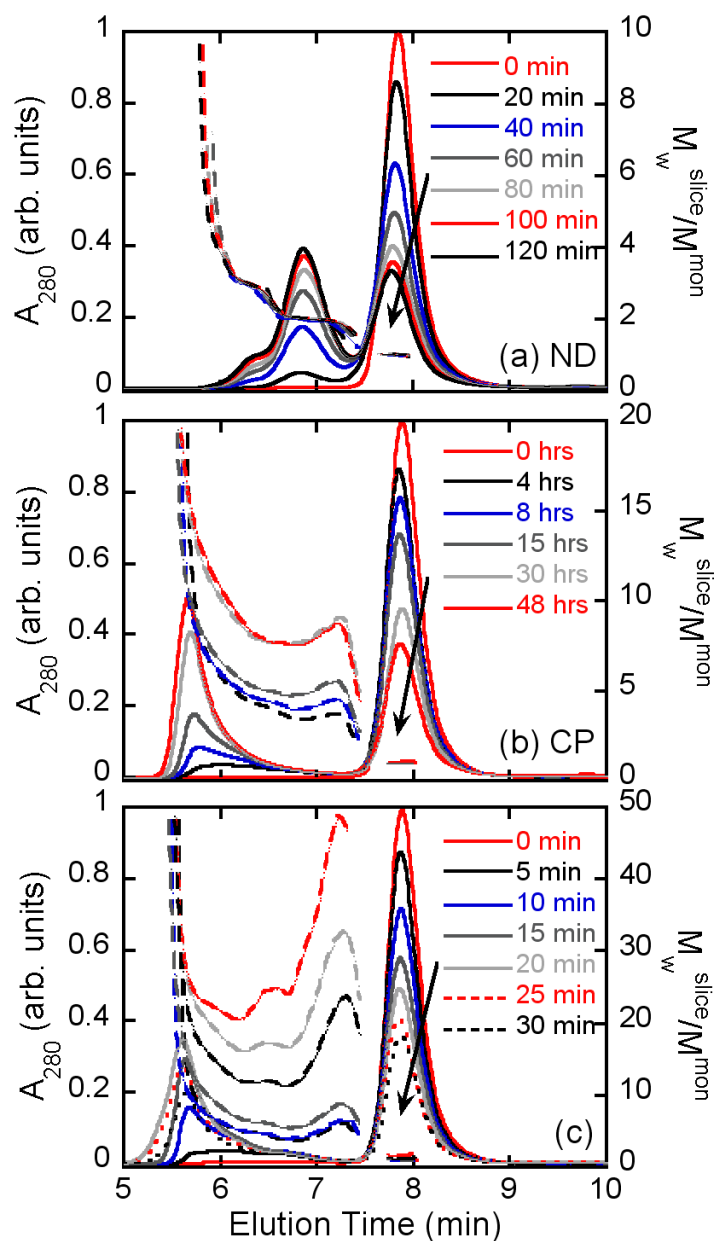


**Figure 3.7** Representative size exclusion chromatograms of different isothermal aggregation mechanisms overlaid with molecular weight data from in-line multi angle light scattering. (a) nucleation dominated growth (pH 4, 0 mM NaCl, 60 °C) (b) growth via chain polymerization (pH 5, 20 mM NaCl, 60 °C) (c) growth initially by (soluble) aggregate-aggregate condensation followed by precipitation / insoluble aggregate formation (pH 5, 500 mM NaCl, 58 °C).

Figure 3.7B shows chromatograms for pH 5, 20 mM NaCl, where aggregates grew to high  $M_w$  but remained soluble, and coeluted in the void of the column. This is seen in the monotonic decrease in the monomer area and increase in the aggregate area in the SEC chromatograms. Figure 3.7C shows the corresponding results for pH 5, 500 mM NaCl, where aggregates grew large and coeluted in the void of the column, but at longer incubation times samples became visibly hazy and precipitates were readily recovered via benchtop centrifugation. For conditions with precipitate present (indicated by dashed curves for the SEC profiles in Figure 3.7C), only the supernatant was injected on SEC-MALS. This resulted in a decrease in the total area of the chromatograms, as seen by inspection of the dashed SEC chromatograms in Figure 3.7C.

While it was relatively simple to identify conditions by visual inspection of SEC when aggregates remained as dimers and small oligomers, as opposed to growth to large aggregates, a different representation of the SEC-MALS data was needed to determine the mechanism by which aggregates grew if they showed significant growth. This is shown in Figure 3.8. The weight average molecular weight, including monomers and aggregates in solution, is denoted by  $M_w^{\text{tot}}/M^{\text{mon}}$ , where the  $M_w^{\text{tot}}$  was calculated by integrating  $M_w$  across the entire chromatogram of peaks containing protein (see also Chapter 2). This value is plotted as a function of the square of extent of reaction in Figure 3.8.

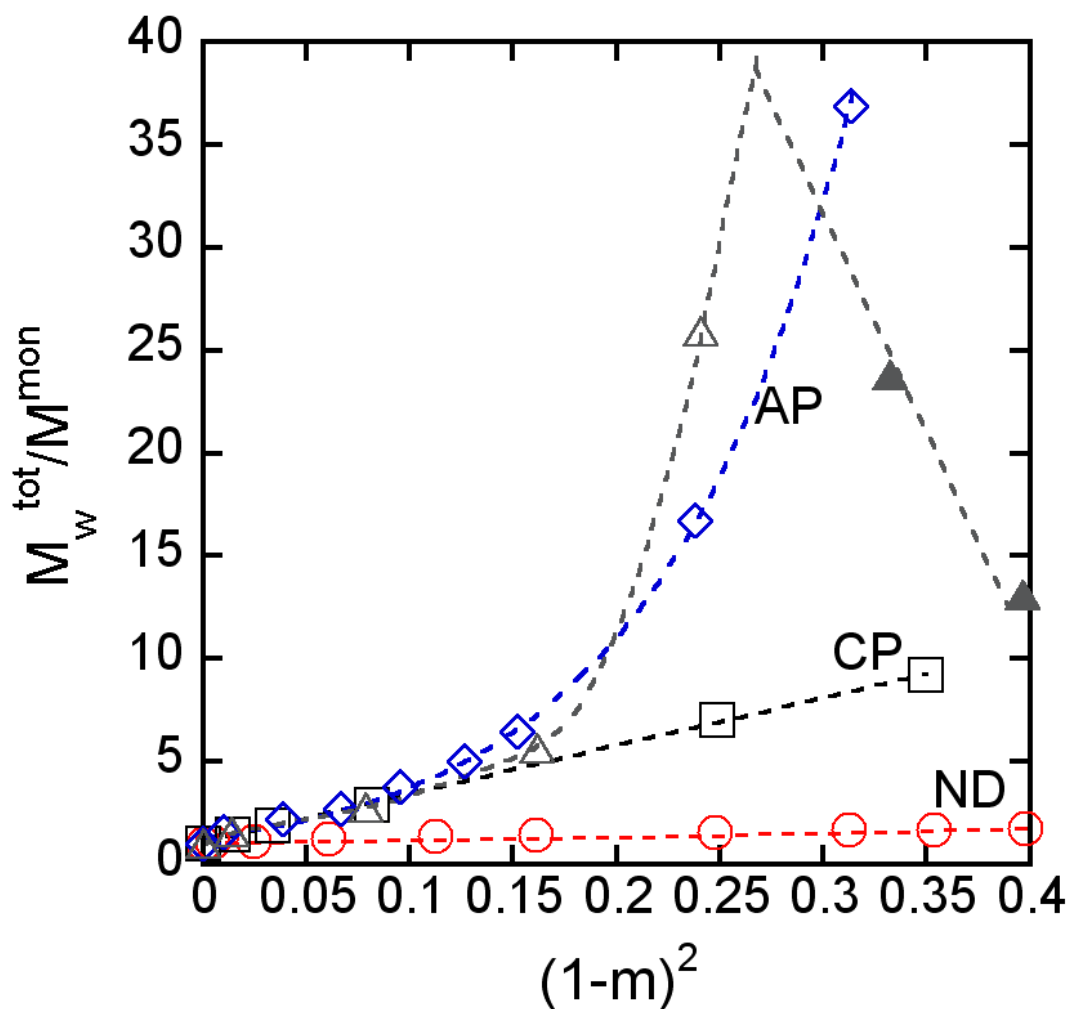


Figure 3.8 Representative plots ( $M_w^{tot}/M_w^{mon}$  vs.  $(1-m)^2$ ) of four aggregation mechanisms observed at different solution conditions. Red circles illustrate nucleation-dominated behavior, where aggregates formed, but did not grow greatly beyond dimers and small oligomers. Black squares show aggregate growth by rapid monomer addition (chain polymerization). Blue diamonds show aggregate growth by a combination of chain polymerization and aggregate-aggregate condensation. Gray triangles show aggregate growth by condensation as soluble species (open triangles) and eventual precipitation removing aggregates from solution (filled triangles). The dotted lines are guides to the eye.

According to theoretical considerations,<sup>38,51</sup> this type of plot shows linear behavior when aggregates grow primarily through monomer addition or, equivalently, chain polymerization (CP). An upturn in these types of plots represents growth of aggregates by aggregate-aggregate condensation polymerization (AP). In addition to these two growth mechanisms, the nucleation dominated (ND) regime was distinguishable as the conditions where there was a linear relationship between  $M_w^{\text{tot}}/M^{\text{mon}}$  and  $(1-m)^2$ , but the aggregates did not reach sizes larger than dimers and small oligomers even as one considered large extents of monomer loss (i.e., high values of  $(1-m)^2$ ).

The gray triangles in Figure 3.8 represent conditions where growth of soluble aggregates was through a hybrid mechanism; aggregate-aggregate condensation polymerization to form soluble aggregates occurred at low extents of monomer loss, but precipitation of at least the highest  $M_w$  aggregates occurred within the first two half-lives tested for Figure 3.8. The final type of aggregate growth mechanism is not represented in Figures 3.7 and 3.8; this is one in which visible haze, particle formation, and/or phase separation (PS) occurred almost immediately upon detectable monomer loss. Due to the small or undetectable amounts of soluble aggregates present in such cases, it was not possible to obtain reliable  $M_w$  data from MALS for those samples.

The growth mechanism at each pH and NaCl concentration was categorized using the analysis illustrated in Figure 3.8 to create a state diagram summarizing how the growth mechanism depends on pH and added NaCl. This diagram is shown in

Figure 3.9. The temperature at which isothermal incubation was monitored is marked next to each of the symbols; as noted above, these align semi-quantitatively with the  $T_{2h}$  values, while maximizing the number of samples that could be incubated simultaneously at the same temperature. The average temperature for incubation in Figure 3.9 is  $60 \pm 3$  °C. The five types of aggregate growth mechanisms are represented by the five symbol types and the labels in Figure 3.9 (see also Figure caption).

Figure 3.9 shows that pH and NaCl concentrations greatly impact the growth mechanism of aggregates. At low pH, even for conditions with appreciable salt concentrations (less than approx. 200 mM), little growth occurred. Increasing pH first resulted in larger aggregates, growing by chain polymerization. At higher pH, aggregates formed visible haze. At higher NaCl concentrations, aggregates were able to grow quickly to high  $M_w$  by condensation to form larger soluble aggregates. In general, addition of NaCl and/or increased pH led to enhanced aggregate-aggregate coalescence (AP or PS mechanism).

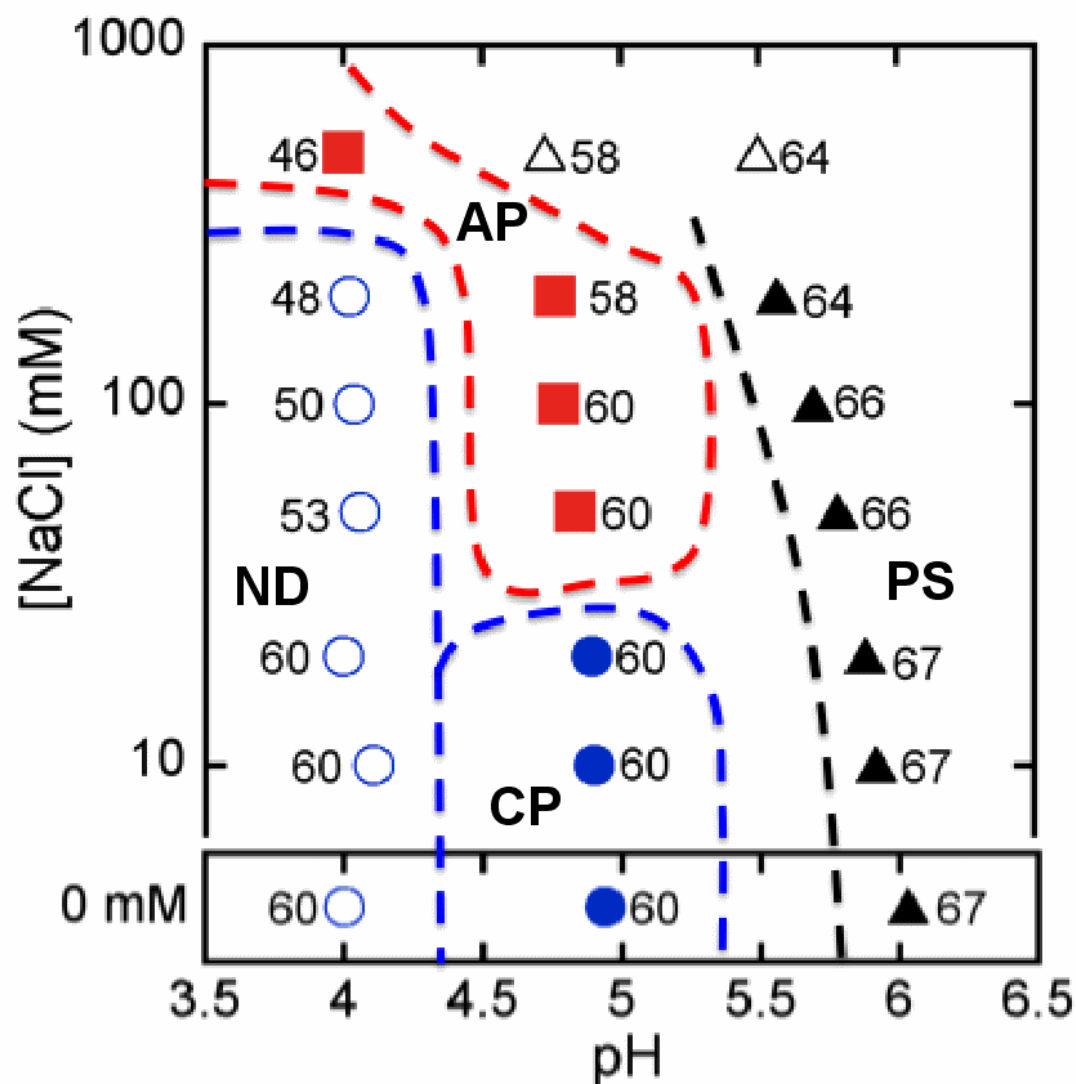


**Figure 3.9** State diagram of aggregation mechanism as a function pH and NaCl concentration. The qualitative aggregation mechanism(s) were monitored over slightly longer incubation times than the first half-life at a given temperatures (indicated by the number label next to each point in the figure). The different mechanisms are indicated by the different symbol types: nucleation dominated (open circles); growth via chain polymerization (filled circles); condensation-dominated growth (squares); condensation followed by macroscopic precipitation / phase separation (open triangles); aggregate precipitation / phase separation (filled triangles).

### 3.5 Reversible aggregate phase separation

Previous studies<sup>26,28</sup> indicated that a reversible phase transition can occur for non-native aggregates (rather than monomers), and that this may help explain the pH and salt dependence of the formation of haze and macroscopic particles. In order to test this hypothesis for antiSA IgG1 aggregates, pH titrations were performed on initially soluble aggregates (see Chapter 2) at 0.5 mg/mL aggregates, corresponding to samples incubated at elevated temperature for 1 half-life, in keeping with the behavior categorized in the state diagram in Figure 3.9.

Figure 3.10 shows a representative pH titration of an initially soluble aggregate sample. In this example, the aggregate concentration was 0.9 mg/mL (1 mg/mL total protein concentration) to make the transition more pronounced for clarity in the figure. As pH was raised, the aggregates phase separated to form white visible haze. Then, as the pH was lowered on the same sample, the suspension dissolved to form a clear solution. SEC before and after the pH titration showed no change in monomer content (not shown). This indicates that the formation of a suspension of visible or large sub-visible particles is, at least in part, a result of reversible phase separation of aggregates. The pH value at which the initial down turn in % transmission occurred (see Chapter 2) was determined at a series of NaCl concentrations. Figure 3.11 shows the pH titrations at the various NaCl concentrations. The transition points are shown as X symbols, connected by a dotted line, in Figure 3.12. This estimated cloud point boundary is overlaid on the state diagram aggregation mechanisms for antiSA IgG1.

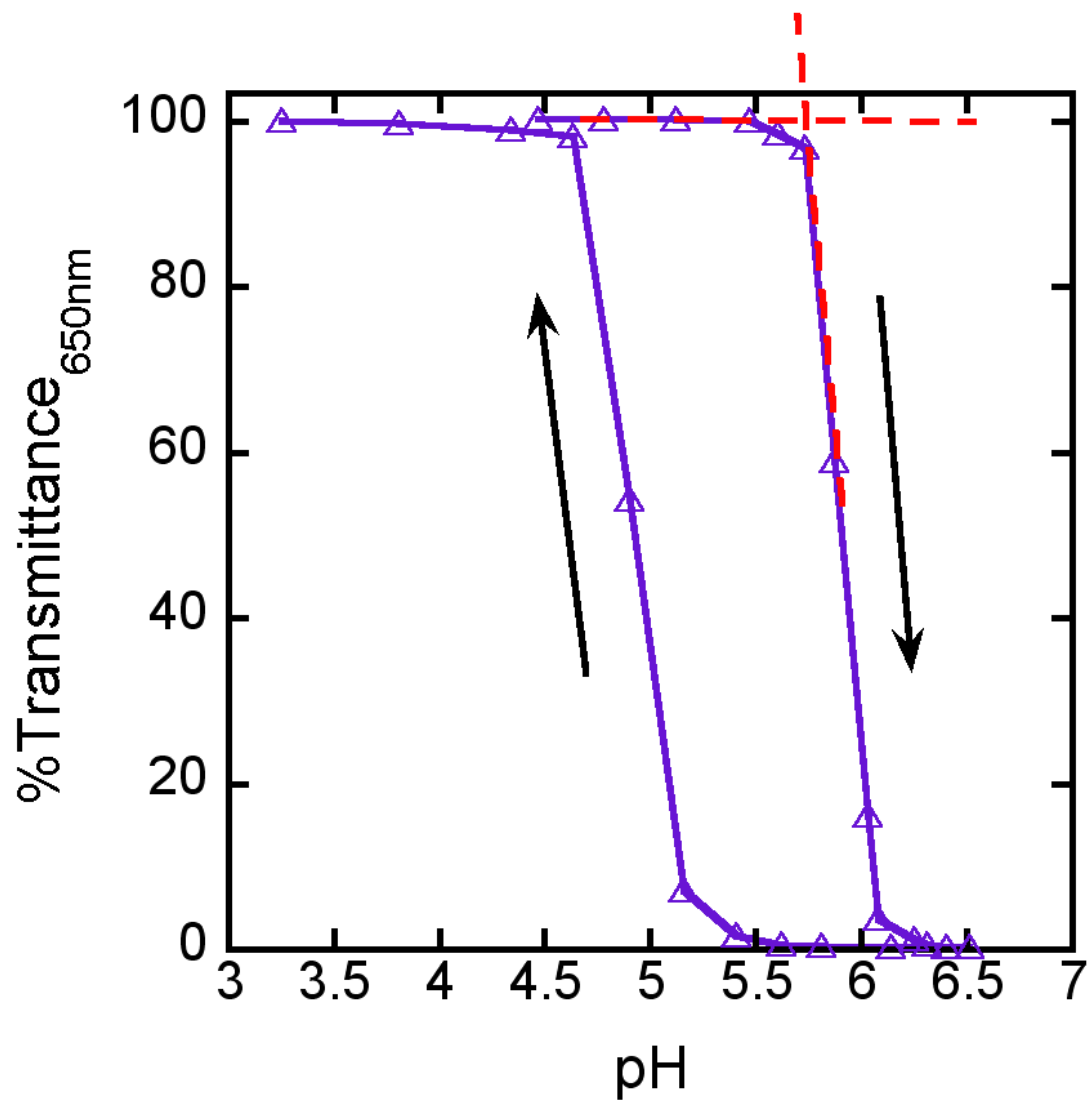


**Figure 3.10** Representative pH titration at room temperature of initially soluble aggregates. The percent transmittance at 650 nm (UV-Vis spectrometry) was used as a measure of turbidity of the solution at each pH step in the titration.

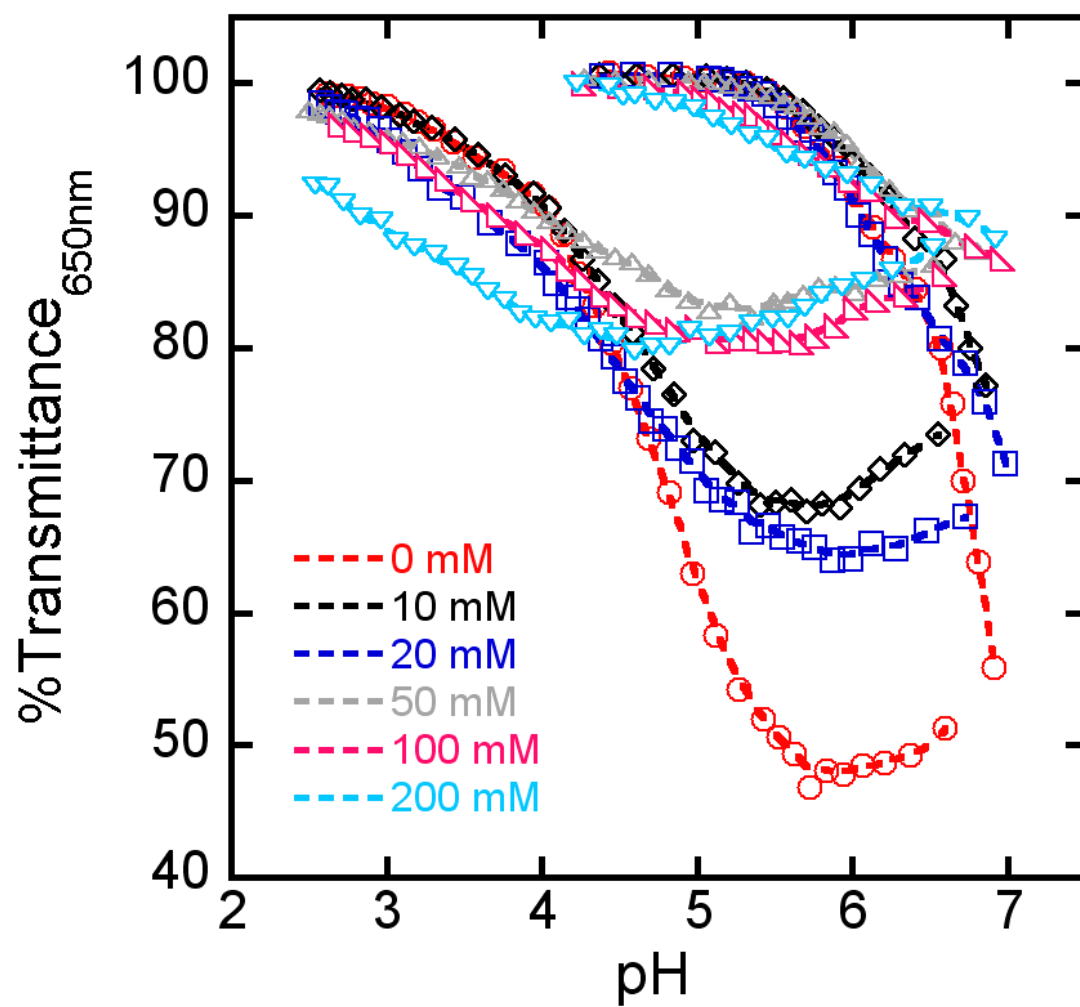


**Figure 3.11** Reversible phase transitions of aggregates with various concentrations of added NaCl. The samples for the pH titration began as 0.5 mg/mL soluble aggregates at pH 4.5.

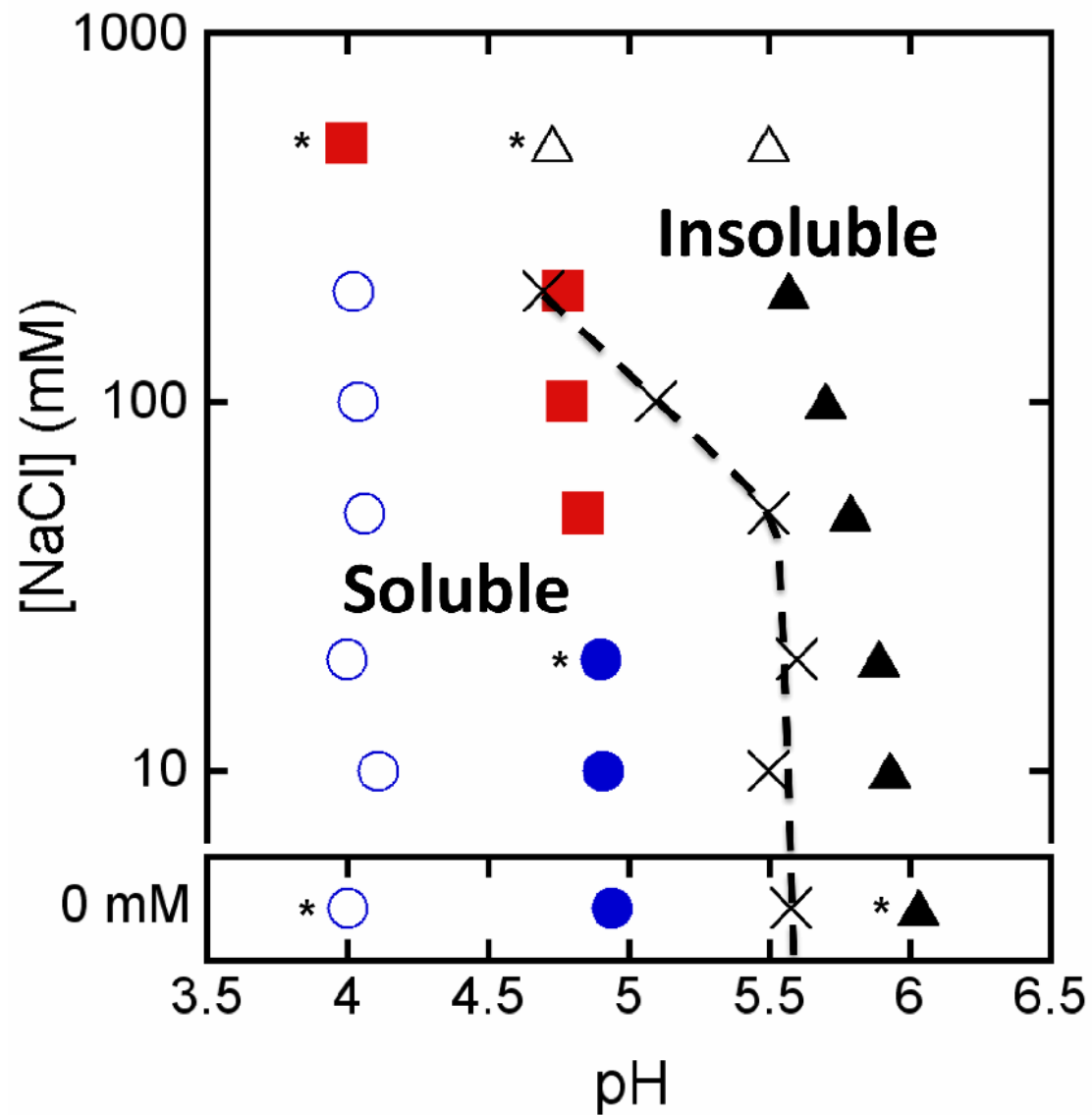


**Figure 3.12** Overlay of the boundary between soluble and phase-separated aggregates (x symbols and dashed line) on the state diagram of qualitative aggregation mechanisms. See main text for additional details. Structural analyses of the resulting aggregates were performed at conditions indicated with asterisks (Figures 3.13-3.15).

### **3.6 Structural changes with aggregation**

Structural changes accompanying aggregation were characterized at five conditions corresponding to the five growth mechanisms, using a combination of spectroscopic techniques that probe secondary structure and/or different measures of tertiary structure, relative to the folded monomer. The conditions chosen for characterization are marked with asterisks in Figure 3.12, corresponding to state points that lie within each of the five regimes in the state diagram. Table 2.1 summarizes the isothermal incubation conditions under which each aggregate sample was created as well as the resulting aggregate content and size, and the growth mechanism or region in Figure 3.9. The assays described in this thesis were only able to measure structures of soluble aggregates. So, pH 6, 0 mM NaCl condition was not measured, because insignificant amounts of soluble aggregates were present at that condition.

#### **3.6.1 Circular dichroism (CD)**

Average secondary structures of each of the conditions that retained more than a few percent soluble aggregates were measured using far-UV circular dichroism (CD). The CD spectra after buffer controls are shown in Figure 3.13A. Monomer controls at each condition are shown as solid lines, and overlay with each other within the resolution of the figure. The dashed colored lines represent aggregated samples. Figure 3.13B shows the corresponding spectra after the contribution from residual

monomer was subtracted (see Chapter 2). For clarity, the average monomer spectrum is shown for comparison to the aggregate-only contributions in Figure 3.13B.

The aggregates that grew by nucleation dominated (ND) and chain polymerization (CP) mechanisms appeared to have the largest changes in their secondary structure, with the negative peak at around 217 nm increased in intensity and width with a slight blue shift in the spectra in Figure 3.13B. The two conditions that grew by aggregate-aggregate condensation polymerization, whether the aggregates remained in solution or eventually phase separated, appeared to have relatively smaller changes in secondary structure compared to monomer. The sample that formed visible particles is not included in Figure 3.13, because the solution contained negligible amounts of soluble aggregate that was detectable by CD.

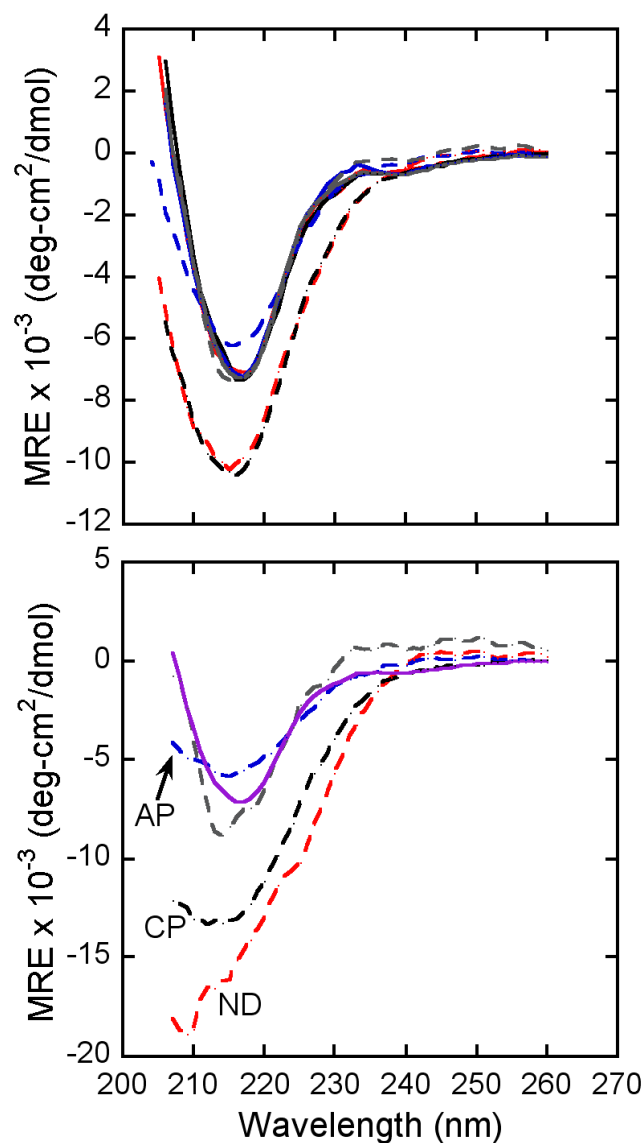


**Figure 3.13** Circular dichroism (CD) spectra for monomer and aggregates at four different conditions corresponding to different regions of the aggregation mechanism state diagram (Figure 3.9). Solid lines correspond to monomer controls. Dashed lines correspond to aggregates formed as summarized in Table 2.1. The bottom panel shows the CD spectra with monomer contributions subtracted from the corresponding full spectrum (including residual monomer) in the top panel. The solid line in the bottom panel is the average of the four monomer spectra in the top plot. Red: nucleation dominated; black: growth by chain polymerization; blue: growth primarily by condensation; gray: growth by condensation and then precipitation.

### 3.6.2 Intrinsic fluorescence (FL)

Intrinsic fluorescence spectra were measured for the same samples as in Figure 3.13, and compared with and without subtraction of the residual monomer contributions. Excitation was at 295 nm to preferentially probe changes in Trp environments. The color and line type scheme are the same as in Figure 3.13. Aggregation, regardless of growth mechanism, resulted in larger intensities and red shifts in the emission spectra, corresponding to greater solvent exposure for at least some Trp residues, and possibly some quenching of Trp fluorescence in the folded monomer state. As in Figure 3.13, the bottom panel in Figure 3.14 shows the emission spectra corrected for monomer contributions; aggregation at low pH and low NaCl (ND conditions) resulted in the largest detected change in Trp exposure, followed by slightly higher pH and NaCl concentration (CP conditions), and finally higher pH and/or NaCl concentration (AP and AP + PS conditions).

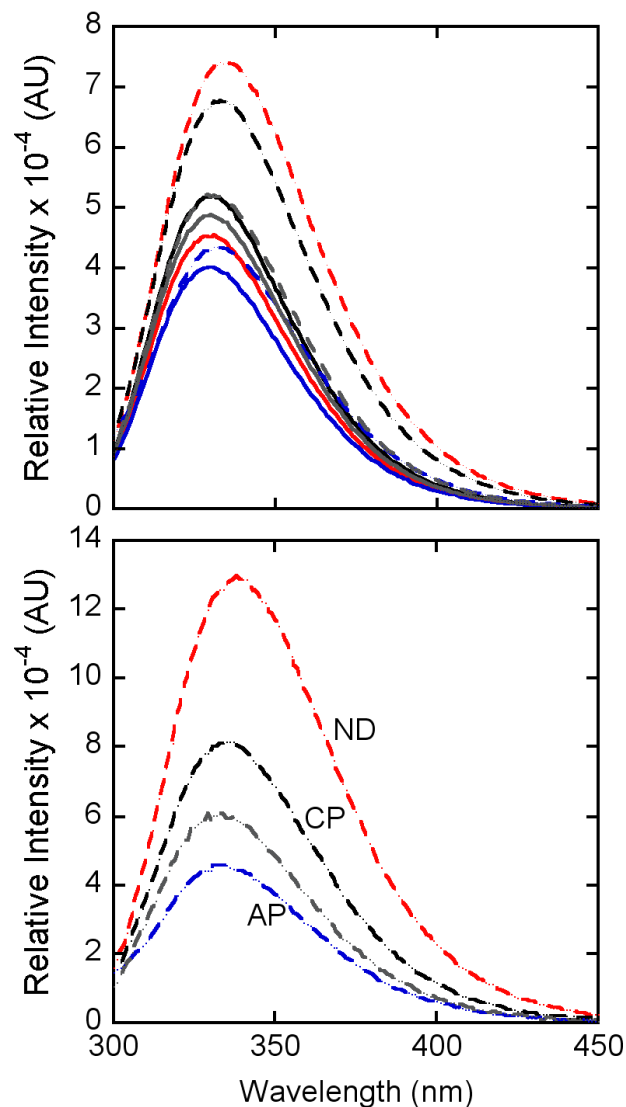


**Figure 3.14 Intrinsic fluorescence spectra showing monomer (solid) and aggregate (dashed) at four different conditions corresponding to different growth mechanisms. The aggregates were formed as summarized in Table 2.1. The excitation wavelength was 295 nm. The bottom panel shows the aggregate spectra after correcting for monomer contributions to the full spectra shown in the top panel. Red: nucleation dominated; black: growth by chain polymerization; blue: growth primarily by condensation of soluble aggregates; gray: growth by condensation followed by precipitation / phase separation.**

### 3.6.3 ThT binding fluorescence

Figure 3.15 shows ThT binding monitored by fluorescence emission for the same sample conditions as in Figures 8 and 9, using the same color and line schemes in the above figures. Similarly, the upper and lower panels in Figure 3.15 show the spectra without and with subtraction of the monomer contributions, respectively. Monomer controls in this case showed negligible binding of ThT, while aggregated samples bound ThT strongly. As in the above figures, samples had different amounts (by mass) of soluble aggregate present, depending on the state point and particular incubation time (see also Table 2.1). Figure 3.15B shows that the ThT binding spectra are virtually indistinguishable, upon correcting for the difference in aggregate content between samples.

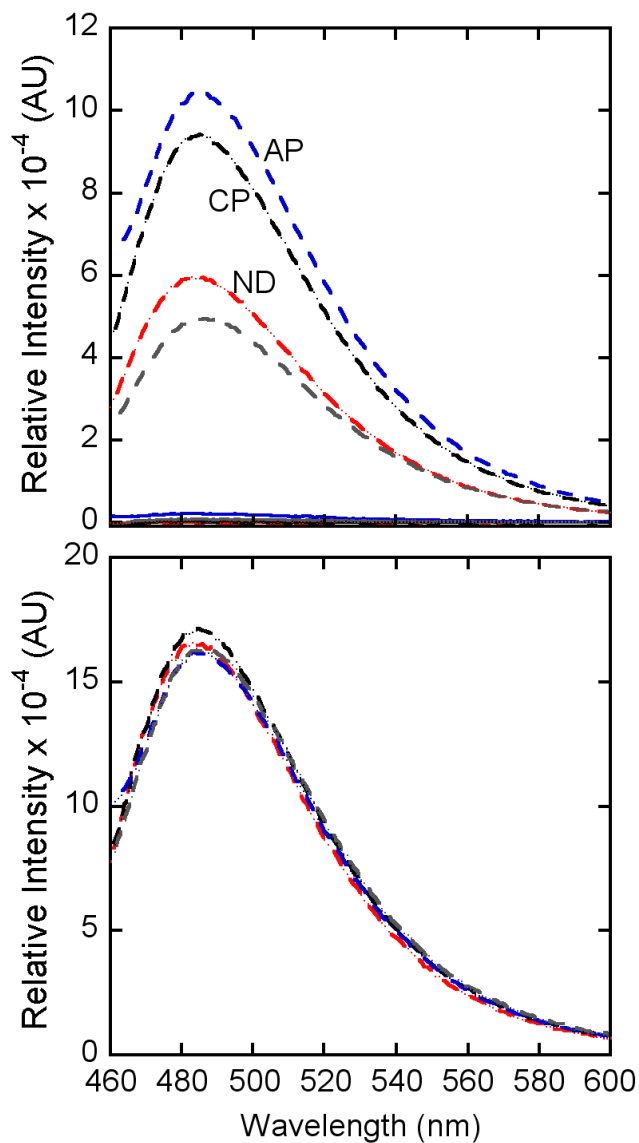


**Figure 3.15 [Top] Thioflavin T (ThT) fluorescence spectra showing negligible binding to monomer (solid curves) and significant binding to aggregates (dashed curves) at the four conditions corresponding to Figure 3.9. Red: nucleation dominated; black: growth by monomer addition; blue: growth by condensation; gray: growth by condensation and then precipitation. ThT binding of early precipitation condition is not shown, as this sample had negligible soluble aggregates in solution. [Bottom] Monomer corrected emission spectra for the four aggregate samples. The color scheme is the same as the top panel. Aggregate samples were formed as summarized in Table 2.1.**

### **3.6.4 Qualitative comparison of structural assays**

Although it is difficult to quantitatively compare what is “large” and what is not, when comparing changes in different spectroscopic techniques, Table 3.2 provides at least a qualitative ranking of the degree of structural perturbation relative to monomer controls, as probed by each technique for the 4 different conditions tested. Note: the rankings are self-consistent within each technique, but should not be compared head to head across techniques. For example, the difference between ranking 1 and 3 for one technique does not necessarily quantitatively correspond to the same degree of difference for ranking 1 and 3 of another technique.

**Table 3.2 Qualitative ranking of structural changes of aggregates formed through different growth mechanisms as measured using different techniques. The most pronounced changes in structure are denoted with 1, with larger numbers indicating relatively less pronounced structural change detected by a given assay. The rankings are only qualitative within a given assay. All aggregate structures were perturbed compared to monomer, based on ThT binding, but binding was indistinguishable among different aggregate preparation conditions.**

<b>Growth Mechanism</b>	<b>CD</b>	<b>Intrinsic Fluo.</b>
Nucleation Dominated (ND)	1	1
Chain Polymerization (CP)	2	2
Agg.-Agg. Condensation Polymerization (AP)	3 or 4	4
Condensation + Phase Separation	3 or 4	3
Precipitation / Phase Separation (PS)	--	--

## Chapter 4

### DISCUSSION

#### 4.1 Aggregation rates show opposite correlations with $T_m$ and $G_{22}$ vs. pH and [NaCl]

Increasing pH and adding NaCl had significant effects on the conformational transitions observed in DSC. With increasing pH,  $T_m$  values of all discernable endotherms shifted to higher temperatures, indicating increased conformational stability of multiple domains. This occurred both with and without added NaCl, but transitions occurred at systematically lower  $T_m$  values with 100 mM NaCl present for a given pH. For pH 4 conditions, this resulted in a more distinguished  $CH_2$  peak. In this case, it was possible to discern more than one endotherm, and the largest-area endotherm corresponded with the onset of aggregation during repeated heating; suggesting Fab unfolding is involved with aggregate formation under those conditions. At higher pH values, only one main endotherm was unambiguously discernable. It is hypothesized that unfolding of multiple domains occurred simultaneously; this includes the aggregation-prone region(s), as that single endotherm was not significantly reversible.

The value of  $G_{22}^*$  is a measure of net colloidal interactions, such as hydrophobic, van der Waals, and electrostatic interactions. At sufficiently low protein

concentration ( $c$ ), there is a simple and exact relationship between  $G_{22}$  and  $B_{22}$ ; specifically  $G_{22} = -2B_{22}$ .<sup>43</sup> Thus, one can semi-quantitatively correlate  $-G_{22}$  with  $B_{22}$ , for readers more familiar with  $B_{22}$ . Any value of  $-G_{22}^*$  above 1 indicates net repulsive interactions greater than what is reasonable to expect based solely on steric interactions, typically due to electrostatic repulsions. Any value below 1 indicates net attractions relative to steric-only interactions, and may be due to a combination of electrostatic and non-electrostatic contributions.

Upon increasing pH at acidic conditions, there was a significant decrease in  $-G_{22}^*$  both with and without added salt for antiSA IgG1. At low pH and ionic strength,  $-G_{22}^*$  was significantly greater than 1, indicating electrostatic repulsions were prominent. At higher pH, or with 100 mM of added NaCl in all cases,  $-G_{22}^*$  was below 1; indicating net attractions relative to steric-only interactions. The effects of added NaCl were most pronounced at low pH, and became effectively negligible with increasing pH. The salt dependence is consistent with strong electrostatic, repulsive interactions at low pH, with weak or negligible contributions from electrostatic repulsions or attractions at higher pH values. Qualitatively, the behaviors summarized above regarding unfolding and colloidal interactions are similar to analogous results for a different IgG1 antibody.<sup>10</sup>

In comparing the effects of pH and added NaCl on conformational stability ( $T_m$ ), colloidal interactions ( $-G_{22}^*$ ), and relative aggregation rates ( $T_{2h}$ ), it was found that aggregation rate is strongly related to conformational stability. The difference between  $T_{2h}$  and  $T_m$  was relatively constant among the six conditions examined. This

is apparent both from inspection of Figure 3.5, and by plotting  $T_{2h}$  versus  $T_m$  (Figure 4.1). Higher  $T_{2h}$  values indicate relatively lower aggregation rates, and this correlates quantitatively with increased conformational stability for antiSA IgG1 as a function of pH and [NaCl]. Figure 3.5 clearly shows that the opposite trend occurs when comparing aggregation rates ( $T_{2h}$ ) and colloidal interactions ( $G_{22}^*$ ). That is, as  $T_{2h}$  rises (lower relative aggregation rates) the colloidal interactions become increasingly attractive; this is the opposite of what one anticipates if colloidal interactions were a strong determinant of aggregation rates.<sup>16,22,52</sup> From a mechanistic perspective, this suggests that the decrease in concentration of (partially) unfolded monomers, due to increased Fab  $T_m$  values, sufficiently offsets the more attractive colloidal interactions as pH is increased for antiSA IgG1. There is also small increase in aggregation rates (decreased  $T_{2h}$ ) with increasing [NaCl] at fixed pH, but this is a much less pronounced effect except at low pH. In that case, added NaCl does cause a large drop in colloidal repulsions, and this may help to explain the increased aggregation rates. This reiterates the importance of simultaneously investigating multiple factors that may determine relative aggregation rates,<sup>22</sup> because different conclusions would have been drawn if only ionic strength was varied at pH 4. As such, it appears that conformational stability is a dominant factor controlling aggregation rates for antiSA IgG1 under most of the conditions considered here, with the exception being conditions of strong electrostatic repulsions.

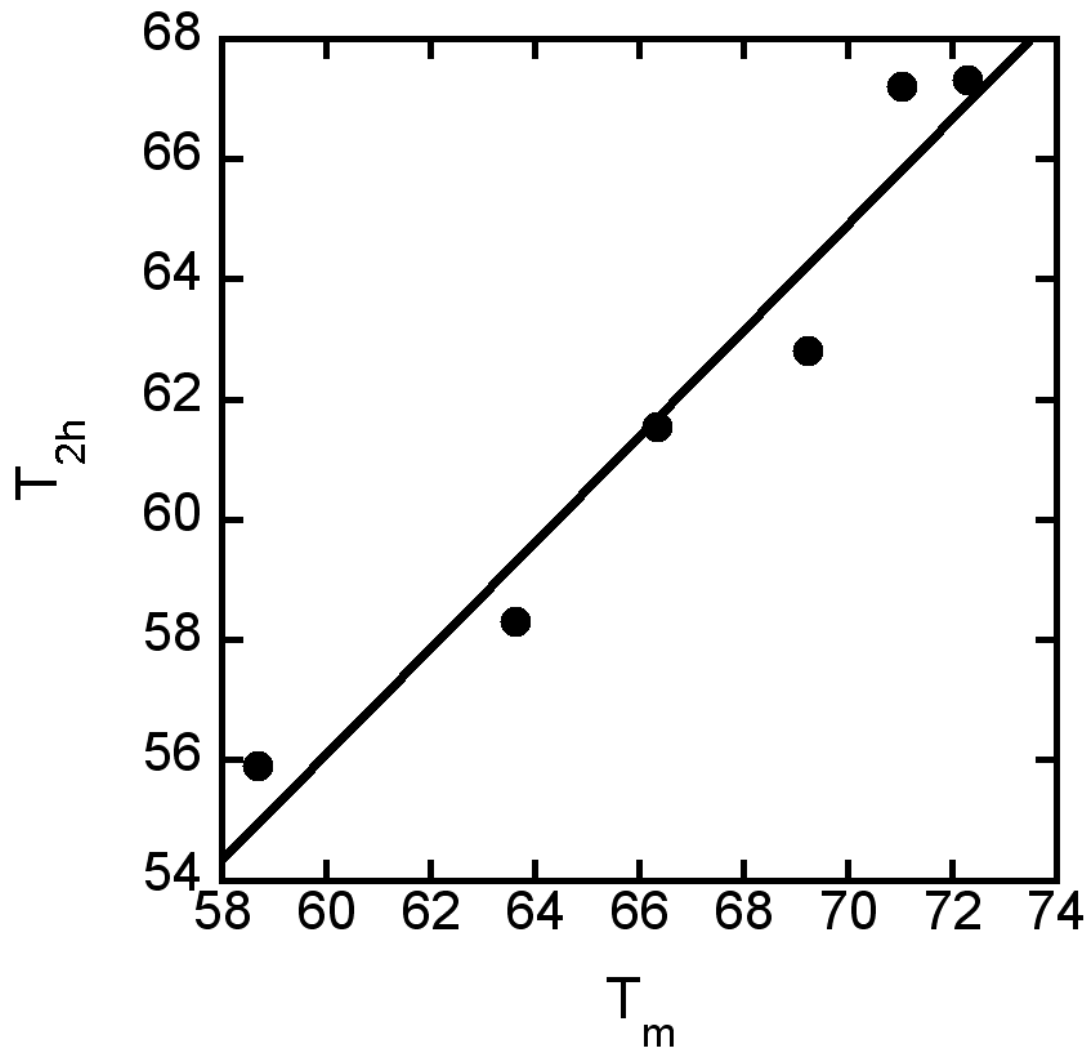


**Figure 4.1 Comparison of interpolated  $T_{2h}$  values from the response surface versus  $T_m$  values corresponding to those in Figure 3.1. There is a linear correlation with an  $r^2$  value of 94.4%. The slope is statistically significant at 0.88 ( $p = 0.001$ ), but the y-intercept is not statistically different from zero ( $b = 3.29$  with  $p = 0.67$ ).**

## 4.2 Combined pH and NaCl effects on aggregation mechanism and formation of insoluble aggregates

The state diagram in Figure 3.9 indicates that aggregate growth mechanism is strongly dependent on pH and [NaCl] at these acidic conditions. At low pH and NaCl concentrations, high net charge of the protein monomers and minimal shielding of these charges result in large inter-molecular repulsions. The strongly repulsive electrostatic interactions resulted in the repulsive  $-G_{22}^*$  value observed at pH 4, 0 mM NaCl, as discussed above. This solution condition also produced aggregates via nucleation dominated (ND) growth, where aggregates formed but did not grow large. The strong electrostatic repulsions may have prevented these aggregates from growing large.

Moving higher in pH and NaCl concentrations produced larger aggregates. Increasing pH towards the pI results in lower electrostatic repulsions as the net charge on the protein decreases. Also, increasing pH increases the buffer-salt ionic strength, which shields the net charge of the molecules, resulting in even lower inter-molecular repulsions. Increasing NaCl concentrations also results in lower electrostatic repulsions as the higher ionic strength allows more shielding of the charge of the proteins molecules. These decreasing electrostatic repulsions may have given rise to the larger aggregates, both soluble and insoluble, which suggests the significant role of inter-molecular repulsions on determining aggregation mechanism.

Overlaying the phase and state diagrams in Figure 3.12 suggests that the kinetic and thermodynamic formations of insoluble aggregates are by the same or similar mechanisms. From the state diagram alone, it appeared that beyond a certain point, condensation was rapid enough for the formation of visible particles. This was verified through the phase diagram, as the line beyond which aggregates were no longer soluble corresponded well with the formation of visible particles from isothermal incubation. This overlap was also previously seen in another IgG1 as a function of pH without added salt.<sup>26</sup> This suggests that the formation of visible particles may be due to a phase separation driven by rapid condensation of aggregates.<sup>5</sup>

The rapid condensation, and thus phase separation of aggregates, is sensitive to changes in electrostatic interactions. Electrostatic interactions become less repulsive at higher pH conditions, where insoluble aggregate formation was observed through kinetically controlled aggregate growth (state diagram) and reversible phase transition of aggregates (pH titrations). This idea is supported by findings of Sahin and coworkers<sup>11</sup> and Li and coworkers<sup>24</sup> that showed that colloidal interactions corresponded well with the formation of insoluble aggregates through thermally accelerated aggregation. Brummitt et al. also demonstrated a strong correlation between  $z^*$  and reversible phase separation of an IgG1,<sup>26</sup> suggesting that lowering the electrostatic repulsions plays a major role in phase behavior of aggregates.

However, a recent study by Kroestsch and coworkers<sup>28</sup> indicates that the decrease in electrostatic repulsions may not be the only factor influencing the phase

separation of aggregates. They probed the same reversible phase behavior of initially soluble aggregates of a small globular protein, aCgn. Through an extensive study, they found that ionic strength and salt type both had an effect on the phase behavior of aggregates, in addition to pH effects.<sup>28</sup> The differences in phase boundary based on salt type indicated that preferential accumulation of some ions on the surface of the protein may affect the phase behavior.<sup>28</sup> Counterion condensation was suggested to affect the phase boundary as well.<sup>28</sup> Such an extensive study for an IgG1 was beyond the scope of this work, but it would be a point of future investigations to determine the effects of other variables, such as salt type, buffer type, and excipients, on the phase behavior of a mAb aggregate.

#### **4.3 Structural changes from aggregation and their possible effect on mechanism of aggregation**

According to far-UV CD and intrinsic fluorescence (Figures 3.13 – 3.14), aggregates that grew in different solution conditions, and thus through different growth mechanisms, displayed varying extents of structure change. Qualitative rankings are tabulated in Table 3.2. These rankings correlate qualitatively with Debye screening lengths at each solution condition except pH 6, 0 mM NaCl, which did not have appreciable amounts of soluble aggregates. Larger Debye length corresponded with greater extent of structural change, with pH 4, 500 mM NaCl (AP) and pH 5, 500 mM NaCl (AP+PS) conditions having similar Debye lengths. This indicates that the

varying amounts of structure change may be a result of intra-aggregate repulsions, as discussed further below.

Intensity of ThT binding, on the other hand, only showed dependence on the concentration of aggregates. This suggests that all the aggregates may have formed amyloid fibrils despite the differences observed through the other assays. A study on the aggregate structure of beta-Lactoglobulin demonstrated that aggregates with seemingly different forms may have the same underlying amyloid fibril structure,<sup>18</sup> suggesting that these aggregates of antiSA may be forming a core of amyloid fibrils independent of growth mechanisms. If ThT binds to cross beta-sheets responsible for forming the “hot spot” core that stabilizes the aggregates, the differences seen in the other assays may not be indicative of mechanistically relevant structural differences.

The structural changes measured through CD and FL may be the result of intra-aggregate repulsions after the formation of the aggregate “core.” As reactive monomers join to form an aggregate, there may be a cross beta-sheet core holding the aggregate together, as indicated by ThT binding. Under some of the conditions, such as pH 4, 0 mM NaCl, the inter-molecular repulsions are large, with large Debye lengths (c. 4 nm). So, the monomeric units in the aggregate are within each other’s Debye screening lengths. This means that the intra-aggregate repulsions are large. As the intra-molecular repulsions in each of the monomers are also large at this condition due to the many positively charged amino acids, these monomeric units may undergo conformation changes to minimize these intra-aggregate and intra-monomer repulsions. This structure change, in combination with high inter-molecular repulsions

(as discussed previously) may be responsible for the aggregates not growing large at this condition, because the “hot spots” for aggregate growth may be less accessible in this new conformation. As the intra-aggregate repulsions and intra-monomer repulsions are lower at the other conditions, less conformational change may be necessary to stabilize the aggregates once they form. This may, in turn, leave the “hot spots” for aggregate growth or condensation more accessible, allowing the larger aggregates to form. These are also the conditions that have less inter-molecular repulsions as well.

The assays used here are globally averaged, with ThT binding being perhaps the least susceptible to this problem since there is almost no binding to native or native-like configurations. Even so, there is no way to discern where within the molecules the structural changes are occurring from any of the assays used here. This highlights the need for caution in overinterpreting global structural assays such as CD and FL (int or extr) when assessing structural changes that may or may not be relevant regarding the mechanisms of aggregation. That notwithstanding, such overall structural changes may still be relevant for the question of aggregate reactivity as described above.

## Chapter 5

### CONCLUSIONS AND FUTURE WORK

This thesis described a global study on the aggregation of a model IgG1 as a function of pH and [NaCl]. Both of these variables were found to strongly influence aggregation rate, mechanism of aggregate growth, aggregate phase behavior, and structure and conformation of aggregates. Varying pH and [NaCl] results in changes in conformational stability and inter-molecular interactions, and these factors were found to influence different aspects of the global aggregation behavior of antiSA IgG1. Relative rate of aggregation, as characterized by T<sub>2h</sub>, correlated strongly with the conformational stability of the protein. Aggregate growth mechanism, phase behavior of aggregates, and global structural change due to aggregation correlated strongly with electrostatic, inter-molecular interactions. Although different global structural changes were observed at various pH and [NaCl] conditions, all forms of aggregates were found to bind ThT, suggesting the formation of amyloid fibrils as the structure at the core of the aggregates.

As pH and [NaCl] are only two of the variables influencing aggregation, a more extensive study would need to be performed to further probe the global aggregation behavior of this model protein. Such factors that would need to be studied are different salt types, added excipients, and protein concentration. Especially studies

at high protein concentrations would be beneficial as therapeutic mAb products are usually formulated at high concentrations.<sup>50</sup>

## REFERENCES

1. Wang, W., Singh, S., Zeng, D. L., King, K. & Nema, S. Antibody structure, instability, and formulation. *Journal of Pharmaceutical Sciences* **96**, 1–26 (2007).
2. Chames, P., Van Regenmortel, M., Weiss, E. & Baty, D. Therapeutic antibodies: successes, limitations and hopes for the future. *British Journal of Pharmacology* **157**, 220–233 (2009).
3. Wei, W. Protein aggregation and its inhibition in biopharmaceutics. *International Journal of Pharmaceutics* **289**, 1–30 (2005).
4. Mahler, H., Friess, W., Grauschopf, U. & Kiese, S. Protein aggregation: Pathways, induction factors and analysis. *Journal of Pharmaceutical Sciences* **98**, 2909–2934 (2009).
5. Weiss IV, W. F., Young, T. M. & Roberts, C. J. Principles, approaches, and challenges for predicting protein aggregation rates and shelf life. *Journal of Pharmaceutical Sciences* **98**, 1246–1277 (2009).
6. Rosenberg, A. S. Effects of protein aggregates: An immunologic perspective. *The AAPS Journal* **8**, E501–E507 (2006).
7. Hermeling, S., Crommelin, D. J. A., Schellekens, H. & Jiskoot, W. Structure-Immunogenicity Relationships of Therapeutic Proteins. *Pharmaceutical Research* **21**, 897–903 (2004).
8. Braun, A., Kwee, L., Labow, M. A. & Alsenz, J. Protein Aggregates Seem to Play a Key Role Among the Parameters Influencing the Antigenicity of Interferon Alpha (IFN- $\alpha$ ) in Normal and Transgenic Mice. *Pharmaceutical Research* **14**, 1472–1478 (1997).
9. Schellekens, H. Factors influencing the immunogenicity of therapeutic proteins. *Nephrology Dialysis Transplantation* **20**, vi3–vi9 (2005).
10. Brummitt, R. K. *et al.* Nonnative aggregation of an IgG1 antibody in acidic conditions: Part 1. Unfolding, colloidal interactions, and formation of high-molecular-weight aggregates. *Journal of Pharmaceutical Sciences* **100**, 2087–2103 (2011).
11. Sahin, E., Grillo, A. O., Perkins, M. D. & Roberts, C. J. Comparative effects of pH and ionic strength on protein–protein interactions, unfolding, and aggregation for IgG1 antibodies. *Journal of Pharmaceutical Sciences* **99**, 4830–4848 (2010).
12. Brych, S. R. *et al.* Characterization of antibody aggregation: Role of buried, unpaired cysteines in particle formation. *Journal of Pharmaceutical Sciences* **99**, 764–781 (2010).

13. Vermeer, A. W. P. & Norde, W. The Thermal Stability of Immunoglobulin: Unfolding and Aggregation of a Multi-Domain Protein. *Biophysical Journal* **78**, 394–404 (2000).
14. Anthony L, F. Protein aggregation: folding aggregates, inclusion bodies and amyloid. *Folding and Design* **3**, R9–R23 (1998).
15. Krishnan, S. *et al.* Aggregation of Granulocyte Colony Stimulating Factor under Physiological Conditions: Characterization and Thermodynamic Inhibition†. *Biochemistry* **41**, 6422–6431 (2002).
16. Chi, E. Y., Krishnan, S., Randolph, T. W. & Carpenter, J. F. Physical Stability of Proteins in Aqueous Solution: Mechanism and Driving Forces in Nonnative Protein Aggregation. *Pharmaceutical Research* **20**, 1325–1336 (2003).
17. Roberts, C. J. Non-native protein aggregation kinetics. *Biotechnology and Bioengineering* **98**, 927–938 (2007).
18. Krebs, M. R. H., Devlin, G. L. & Donald, A. M. Amyloid Fibril-Like Structure Underlies the Aggregate Structure across the pH Range for  $\beta$ -Lactoglobulin. *Biophysical Journal* **96**, 5013–5019 (2009).
19. Kendrick, B. S. *et al.* Aggregation of recombinant human interferon gamma: Kinetics and structural transitions. *Journal of Pharmaceutical Sciences* **87**, 1069–1076 (1998).
20. Grillo, A. O. *et al.* Conformational Origin of the Aggregation of Recombinant Human Factor VIII†. *Biochemistry* **40**, 586–595 (2000).
21. Goldberg, D. S., Bishop, S. M., Shah, A. U. & Sathish, H. A. Formulation development of therapeutic monoclonal antibodies using high-throughput fluorescence and static light scattering techniques: Role of conformational and colloidal stability. *Journal of Pharmaceutical Sciences* **100**, 1306–1315 (2011).
22. Roberts, C. J., Das, T. K. & Sahin, E. Predicting solution aggregation rates for therapeutic proteins: Approaches and challenges. *International Journal of Pharmaceutics* **418**, 318–333 (2011).
23. He, F., Woods, C. E., Becker, G. W., Narhi, L. O. & Razinkov, V. I. High-throughput assessment of thermal and colloidal stability parameters for monoclonal antibody formulations. *Journal of Pharmaceutical Sciences* **100**, 5126–5141 (2011).
24. Li, Y., Ogunnaiké, B. A. & Roberts, C. J. Multi-variate approach to global protein aggregation behavior and kinetics: Effects of pH, NaCl, and temperature for  $\alpha$ -chymotrypsinogen A. *Journal of Pharmaceutical Sciences* **99**, 645–662 (2010).
25. Hoyer, W. *et al.* Dependence of  $\alpha$ -Synuclein Aggregate Morphology on Solution Conditions. *Journal of Molecular Biology* **322**, 383–393 (2002).
26. Brummitt, R. K., Nesta, D. P., Chang, L., Kroetsch, A. M. & Roberts, C. J. Nonnative aggregation of an IgG1 antibody in acidic conditions, part 2: Nucleation and growth kinetics with competing growth mechanisms. *Journal of Pharmaceutical Sciences* **100**, 2104–2119 (2011).

27. Li, Y., Mach, H. & Blue, J. T. High throughput formulation screening for global aggregation behaviors of three monoclonal antibodies. *Journal of Pharmaceutical Sciences* **100**, 2120–2135 (2011).
28. Kroetsch, A. M., Sahin, E., Wang, H.-Y. & Roberts, C. J. Relating Particle Formation to Salt- and pH-Dependent Phase Separation of Non-Native Aggregates of  $\alpha$ -Chymotrypsinogen A. *in preparation*
29. Sahin, E. *et al.* Aggregation and pH–temperature phase behavior for aggregates of an IgG2 antibody. *Journal of Pharmaceutical Sciences* doi:10.1002/jps.23056
30. Fast, J. L., Cordes, A. A., Carpenter, J. F. & Randolph, T. W. Physical Instability of a Therapeutic Fc Fusion Protein: Domain Contributions to Conformational and Colloidal Stability. *Biochemistry* **48**, 11724–11736 (2009).
31. Andersen, C. B., Manno, M., Rischel, C., Thórólfsson, M. & Martorana, V. Aggregation of a multidomain protein: A coagulation mechanism governs aggregation of a model IgG1 antibody under weak thermal stress. *Protein Science* **19**, 279–290 (2010).
32. Zhang, A., Singh, S. K., Shirts, M. R., Kumar, S. & Fernandez, E. J. Distinct Aggregation Mechanisms of Monoclonal Antibody Under Thermal and Freeze-Thaw Stresses Revealed by Hydrogen Exchange. *Pharmaceutical Research* **29**, 236–250 (2011).
33. Franey, H., Brych, S. R., Kolvenbach, C. G. & Rajan, R. S. Increased aggregation propensity of IgG2 subclass over IgG1: Role of conformational changes and covalent character in isolated aggregates. *Protein Science* **19**, 1601–1615 (2010).
34. Bee, J. S., Davis, M., Freund, E., Carpenter, J. F. & Randolph, T. W. Aggregation of a monoclonal antibody induced by adsorption to stainless steel. *Biotechnology and Bioengineering* **105**, 121–129 (2010).
35. Thirumangalathu, R. *et al.* Silicone oil- and agitation -induced aggregation of a monoclonal antibody in aqueous solution. *Journal of Pharmaceutical Sciences* **98**, 3167–3181 (2009).
36. Kim, N. *et al.* Salt- and pH-Dependent Mechanisms of Non-Native Aggregation of Anti-Streptavidin Immunoglobulin Gamma-1. *In preparation*
37. Li, Y., Weiss IV, W. F. & Roberts, C. J. Characterization of high-molecular-weight nonnative aggregates and aggregation kinetics by size exclusion chromatography with inline multi-angle laser light scattering. *Journal of Pharmaceutical Sciences* **98**, 3997–4016 (2009).
38. Sahin, E. & Roberts, C. J. Size-Exclusion Chromatography with Multi-Angle Light Scattering (SEC-MALS) for Elucidating Protein Aggregation Mechanisms: Overview Chapter. *In Press* (2012).
39. Andrews, J. M. & Roberts, C. J. Non-Native Aggregation of  $\alpha$ -Chymotrypsinogen Occurs through Nucleation and Growth with Competing Nucleus Sizes and Negative Activation Energies<sup>†</sup>. *Biochemistry* **46**, 7558–7571 (2007).
40. Privalov, P. L. Stability of proteins: small globular proteins. *Adv. Protein Chem.* **33**, 167–241 (1979).

41. Brummitt, R. K., Nesta, D. P. & Roberts, C. J. Predicting accelerated aggregation rates for monoclonal antibody formulations, and challenges for low-temperature predictions. *Journal of Pharmaceutical Sciences* **100**, 4234–4243 (2011).
42. Winsor, C. P. The Gompertz Curve as a Growth Curve. *Proceedings of the National Academy of Sciences of the United States of America* **18**, 1–8 (1932).
43. Blanco, M. A., Sahin, E., Li, Y. & Roberts, C. J. Reexamining protein–protein and protein–solvent interactions from Kirkwood-Buff analysis of light scattering in multi-component solutions. *The Journal of Chemical Physics* **134**, 225103–225103–12 (2011).
44. Asthagiri, D., Paliwal, A., Abras, D., Lenhoff, A. M. & Paulaitis, M. E. A Consistent Experimental and Modeling Approach to Light-Scattering Studies of Protein-Protein Interactions in Solution. *Biophys J* **88**, 3300–3309 (2005).
45. Garber, E. & Demarest, S. J. A broad range of Fab stabilities within a host of therapeutic IgGs. *Biochemical and Biophysical Research Communications* **355**, 751–757 (2007).
46. Ionescu, R. M., Vlasak, J., Price, C. & Kirchmeier, M. Contribution of variable domains to the stability of humanized IgG1 monoclonal antibodies. *Journal of Pharmaceutical Sciences* **97**, 1414–1426 (2008).
47. Remmele, Bhat, S. D., Phan, D. H. & Gombotz, W. R. Minimization of Recombinant Human Flt3 Ligand Aggregation at the T<sub>m</sub> Plateau: A Matter of Thermal Reversibility. *Biochemistry* **38**, 5241–5247 (1999).
48. Ginsburg, A. Reversible, Thermally Induced Domain Unfolding in Oligomeric Proteins. Spectral and DSC measurements. *Journal of Thermal Analysis and Calorimetry* **61**, 425–436 (2000).
49. Ogunnaike, B. A. *Random Phenomena: Fundamentals of Probability and Statistics for Engineers*. (CRC Press: 2009).
50. Yadav, S., Shire, S. J. & Kalonia, D. S. Factors affecting the viscosity in high concentration solutions of different monoclonal antibodies. *Journal of Pharmaceutical Sciences* **99**, 4812–4829 (2010).
51. Li, Y. & Roberts, C. J. Lumry–Eyring Nucleated-Polymerization Model of Protein Aggregation Kinetics. 2. Competing Growth via Condensation and Chain Polymerization. *J. Phys. Chem. B* **113**, 7020–7032 (2009).
52. Kumar, V., Dixit, N., Zhou, L. (Lisa) & Fraunhofer, W. Impact of short range hydrophobic interactions and long range electrostatic forces on the aggregation kinetics of a monoclonal antibody and a dual-variable domain immunoglobulin at low and high concentrations. *International Journal of Pharmaceutics* **421**, 82–93 (2011).